

Aeolian dust and diatoms at Roosevelt Island (Ross Sea, Antarctica) over the last two millennia reveal the local expression of climate changes and the history of the Ross Sea polynya.

5 Serena Lagorio^{1,2}, Barbara Delmonte¹, Dieter Tetzner³, Elisa Malinverno¹, Giovanni Baccolo^{1,4}, Barbara Stenni², Massimo Frezzotti⁴, Valter Maggi¹, Nancy Bertler^{5,6}.

¹University Milano-Bicocca, DISAT – Dept. Earth and Environmental Sciences, Milano, Italy

²Ca' Foscari of Venice, Department of Environmental Sciences, Informatics and Statistics, Mestre (Venezia), Italy

10 ³BAS, British Antarctic Survey, High Cross, Madingley Road, Cambridge, CB23 7XT, UK

⁴University Roma Tre, Dept. of Sciences, Geological Science Section, Roma, Italy

⁵Antarctic Research Centre, Victoria University of Wellington, Wellington, 6012, New Zealand

⁶GNS Science, National Ice Core Laboratory, Lower Hutt, 5040, New Zealand

15 *Correspondence to: Barbara Delmonte (barbara.delmonte@unimib.it)*

Abstract.

The pattern of atmospheric and climate changes recorded by coastal Antarctic ice core sites and the processes they illustrate highlight the importance of multiproxy studies on ice cores drilled from such peripheral areas, where regional to local-scale processes can be documented. Here, we present a 2000 year long record of aeolian mineral dust and diatoms windblown to the

20 Roosevelt Island, obtained from the RICE (Roosevelt Island Climate Evolution project) ice core. Mineral dust and diatoms are highly complementary at RICE since they are related to the large-scale South Pacific atmospheric circulation regime, carrying dust-rich air masses that travelled above the marine boundary layer, and local oceanic aerosol transport by low-level marine air masses, respectively. The 550-1470 CE period is characterized by enhanced mineral dust transport originating from the Southern Hemisphere continents, reduced sea-ice extent in the Eastern Ross and Amundsen Seas, and more frequent

25 penetration of humid air masses responsible for the relative increase in snow accumulation. We observe that around 1300 CE, in concomitance with marked El Niño-like conditions, the Ross Sea dipole reaches its maximum expression. After 1470 CE, relatively lower dust and snow deposition at RICE suggests an increase in pack ice in the Eastern Ross and Amundsen Seas. This period is characterized by prominent peaks of aeolian diatoms that are unprecedented over the last 2 kyr, indicating a rapid reorganization of atmospheric circulation. Data suggest an eastward enlargement of the Ross Sea polynya culminating

30 with the opening of the proposed Roosevelt Island polynya, and an increased influence of low-level marine air masses to the site during the Little Ice Age.

The assessment of climatic and environmental variability over the Common Era (CE, the last 2000 years before present; 2 ka BP) is fundamental to place industrial-era warming into the context of natural climatic variability (e.g. IPCC 2021, Smerdon & Pollack, 2016). Based on palaeoclimatic records from Europe, North America and from the extratropical Northern Hemisphere, several climatic periods have been defined and investigated within the past 2,000 years (2 ka). These include, for example, the so-called “Roman Warm Period” (ca. 1-300 CE, Ljungqvist, 2010) and the “Dark Ages Cold Period” (ca. 400-765 CE, Helama et al., 2017) during the first millennium of the CE. The last millennium is characterized by the “Medieval Warm Period” (MWP), also known as “Medieval Climate Anomaly” (MCA) typically associated with warm temperatures between about 800 and 1200 CE (Lamb, 1965; Mann et al., 2009; Bradley et al., 2003). The most prominent episode that occurred during the last 2 ka is probably the “Little Ice Age” (LIA), due to its centuries-long cold climate state leading to glacial advances in many locations worldwide (Matthews & Briffa, 2005). The timing and duration of the LIA, however, cannot be precisely defined since the timing, magnitude and regional expression of the LIA exhibit strong regional variations (Jones and Mann, 2004). The post-industrial period (1850 CE-present) is the last of these periods; it is largely recognized to be the warmest period of the past two millennia and to have a strong anthropogenic influence (IPCC, 2021).

The most pronounced characteristic of the anthropogenic warming is its global reach. Conversely, earlier climate swings of the preindustrial CE lack spatial and temporal coherence, and did not produce globally-synchronous temperature changes at multidecadal and centennial timescales (PAGES2k Consortium, 2017). At the scale of the Antarctic continent, a comprehensive ice core-based analysis of climate variability over the last 2000 years (Stenni et al., 2017) highlights a very complex picture with marked differences in regional trends. As an example, the cooling trend registered prior to 1900 CE at sites such as WAIS Divide and in the region of Victoria Land is in apparent disagreement with the water stable isotope record from coastal, low-elevation sites such as Roosevelt Island, located in between the two (fig. 1). There, increasing rather than decreasing water stable isotope anomalies are registered over that period (Bertler et al., 2018). The origin of such differences arise from the intrinsic sensitivity of coastal sites to register regional-to-local atmospheric signals that are often deeply influenced by maritime air masses. By masking the regional longer-term temperature trends, the marine influence allows obtaining high-resolution records of regional/subregional-scale atmospheric variability that sensitively capture the climate and the environmental history of the Southern Ocean (Masson et al., 2000; Stenni et al., 2017; Bertler et al., 2018).

In this work, we present and discuss new records of aeolian dust and diatoms obtained from the RICE (Roosevelt Island Climate Evolution project) ice core for the last 2 ka, providing an excellent opportunity to assess the climate and the atmospheric processes occurring in the Eastern Ross Sea (ERS, the region within the Ross Sea that stretches towards West Antarctica) over the last two millennia. We address three specific questions: (1) What can mineral dust and windblown diatoms tell us about climatic and atmospheric conditions experienced on Roosevelt Island over the last 2 ka? (2) What climatic and environmental conditions did RICE experience during the last millennium, in particular during the MCA and LIA? How do

the diatom and dust records fit into the much wider Ross Sea context? By defining the local expression of climate swings that occurred at RICE and the way they are connected to other local/regional changes, we aim to provide comprehensive insights of the recent climate evolution in the Ross Sea area, regional sea-ice variability and Ross Sea polynya dynamics, as well as air mass circulation driven by large-scale climatic drivers.

1.1 Insoluble impurities in the context of Roosevelt Island

1.1.1 Mineral dust

75

The RICE ice core, thanks to its relatively high snow accumulation rate (25 ± 2 cm water equivalent yr^{-1} over the last 2700 years, Winstrup et al., 2019) compared to East Antarctic Plateau sites, provides a unique opportunity to study the coastal Eastern Ross Sea (ERS) and to determine the response of the regional atmospheric circulation to key climatic drivers. Indeed, the Ross Sea region is known to be influenced by dynamics affecting both West and East Antarctica, and by oceanic processes.

80 Insoluble impurities found in the RICE ice core mainly consist of mineral dust particles, sourced from New Zealand, southern South America and Australia (Neff & Bertler, 2015). Exposed ice-free areas of West Antarctica also contribute to the dust input at RICE, as deduced by Winton et al. (2016a) on the basis of mineral dust geochemistry and grain size. Although in most East Antarctic sites the concentration of dissolved calcium ions can be used as proxy for a terrestrial source (e.g. Wolff et al., 2010), at RICE the soluble calcium comes primarily from a marine source during the Holocene, and therefore other elements of typical crustal origin such as iron (Fe), aluminum (Al) and manganese (Mn) are better indicators for dust input at the site (Tuohy et al., 2015; Winstrup et al., 2019). The analysis of these elements showed that the seasonal dust pattern is synchronous with black carbon, with a slight tendency to peak in austral summer. However, the annual variability of the dust concentration signal (and related elements) in the snow is quite complex because it is related to three basic and independent factors: (1) atmospheric transport, (2) the availability of fine particles at the dust source and (3) the depositional regime (Delmonte et al., 2017). Crustal elements, such as Fe and Al, tend to display one or two intra-annual peaks at RICE, generally occurring in early-to-late austral winter, while Mn generally peaks in early austral summer, demonstrating that the timing of intra-annual peaks is not always consistent among dust-related elements (Tuohy et al., 2015).

Based on elemental analyses on snow pits, Tuohy et al. (2015) observed a negative correlation between crustal elements and snow density at RICE, suggesting that the highest dust concentration levels can be generally associated with large precipitation related to storm events. It follows from this evidence that dust is deposited at Roosevelt Island mostly through wet deposition during snowfalls. However, the concentration of insoluble particulate material between 1 and $10 \mu\text{m}$ at RICE obtained from a 2-year snowpit (2011-2012 CE, Winton et al., 2016b) shows that dust deposition in the snow pit is episodic, with two annual impurity maxima corresponding to austral spring-summer, while the lowest dust levels are observed in austral winter months. Again, the scenario appears complex because episodic dust events have also been observed in austral winter (Winton et al., 2016b). In Antarctica, austral spring-summer dust maxima and austral winter dust concentration minima have been observed

100

at GV7, (Caiazzo et al., 2017), at Berkner Island, that is an ice rise surrounded by the Filchner-Ronne Ice Shelf (Bory et al., 2010), and at South Pole (Legrand and Kirchner, 1988) (fig. 1).

1.1.2 Aeolian diatoms

105

Although windblown mineral dust aerosol quantitatively represents the most important component of insoluble impurities archived in ice and snow (Delmonte et al., 2013), a quantitatively small but critical fraction of insoluble impurities is represented by other materials, among which are diatoms. Diatoms are single-celled algae (Bacillariophyta) generally light and aerodynamic and thus easily transportable over long-distances by winds (Allen et al., 2020). Diatoms live and prosper in different marine, nonmarine and brackish environments all around the world. When the degree of preservation of individual specimens allows recognizing some species-specific characteristics, the species identification is possible and can aid in identifying potential source regions. Once the source environment is identified, aeolian diatoms preserved in ice core layers can be used as proxy for atmospheric transport pathways complementary to mineral dust (Kellogg & Kellogg, 2005; Burckle et al., 1988). Atmospheric circulation allows a continuous transport of diatoms across Antarctica. However, diatom sources, transport and deposition mechanisms may be geographically different. This implies that the paleoenvironmental significance of the diatom record is different from one glaciological context to another. As an example, in remote high-altitude East Antarctic locations such as Dome C, Vostok (Burckle et al., 1988) and Dome B (Delmonte et al., 2017), the aeolian diatoms allowed to reassess the role of the Patagonian continental shelf at the time of sea level low stand during the last glacial period (Delmonte et al., 2017). This because the most important diatom sources in these isolated remote sites are the exposed diatom-bearing terrestrial sediments containing marine and nonmarine diatoms (Burckle et al., 1988). In other East Antarctic locations such as Talos Dome for example, located on the periphery of the Antarctic Plateau close to the Transantarctic Mountains (Delmonte et al., 2013), aeolian diatoms mainly derive from reworked subaerially-exposed sediments. Indeed, diatom frustules represent a pervasive component of Antarctic sediments in Victoria Land even at altitude above 2000 m a.s.l. (McKay et al., 2008), and they can be easily remobilized by winds from exposed sediments or subaerially-exposed dry source beds. In South Pole ice, marine and nonmarine species have been observed (Kellogg & Kellogg, 2005). As the surface Antarctic wind field is dominated by katabatic outflow towards the sea with occasional large storm penetration (Bromwich and Robasky 1993), marine diatoms are believed to be carried by these episodic events. A systematic study of diatom concentration in the South Pole ice core over the last 2 ka BP revealed that the concentration of diatoms varied between 0 and >450 valves per Liter, and their variability was related to climate conditions with the highest abundances mainly occurring during the LIA (1400-1750 CE) (Kellogg & Kellogg, 1996). More recently, Tetzner et al. (2022a, 2022b) showed through a multi-site approach that diatom species and their seasonal variability vary between coastal, low elevation sites and continental, high elevation sites of the Antarctic Peninsula. While the former display a marked seasonal signal dominated by species like *Fragilariopsis cylindrus* and *F. curta*, typically sourced from the Southern Ocean seasonal sea-ice zone, the latter display a higher proportion of open ocean diatoms that are more distally-sourced and lack of a clear seasonality. Thus, the authors proposed that the geographically

110

115

120

125

130

135 and temporally-variable diatom signal preserved in ice and snow samples from the Antarctic peninsula can be exploited to recover significant environmental information from both the sea-ice zone and the open ocean. In this context, the presence of polynyas, that are areas of open water surrounded by sea ice, can play a major role. This because polynyas are regions of enhanced oceanic primary and secondary productivity where the growth of phytoplankton biomass, including diatoms, is greater than in adjacent waters (Park et al., 2018).

140 The Ross Sea polynya is the largest regularly forming polynya around Antarctica. It waxes and wanes between May and October, but mostly develops from early austral spring, until reaching the frontal sea ice margin by January (Arrigo and van Dijken, 2003). In the Ross Sea polynya, phytoplankton blooms peak in early austral summer, declining afterwards in the late austral summer season prior to refreezing (Arrigo and van Dijken, 2003). With an average winter area around $20.23 \times 10^3 \text{ km}^2$ becoming about $396.5 \times 10^3 \text{ km}^2$ in austral summer (Arrigo and Van Dijken, 2003), the wind-driven latent heat polynya of the

145 Ross Sea plays an important role in sea ice production, as older sea ice is continually blown offshore and replaced by newly-formed frazil ice.

1.2 Stable water isotopes and snow accumulation at RICE

150 The ice core stable water isotope record at Antarctic coastal sites is typically sensitive not only to air temperature but also atmospheric circulation and sea ice extent (Bertler et al., 2018). Bertler et al. (2018) provide evidence that the deuterium record at RICE is positively correlated with surface air temperature at the site which, in turn, is representative of surface air temperature variability across the Ross Ice Shelf and Ross-Amundsen Sea, as well as Western Marie Byrd Land. Also, the Siple Dome site (fig. 1) is within the area of statistically-significant temperature correlation with RICE, while conversely that

155 is not the case for WAIS Divide. Also, there is no correlation between RICE surface air temperature and the westernmost margin of the Transantarctic Mountains.

The δD stable water isotope composition of RICE snow layers is also negatively correlated with sea-ice concentration (SIC) in the Eastern Ross Sea (ERS) and Northern Amundsen Sea (AS), suggesting that less depleted isotope values reflect air mass and humidity advection from the nearby Ross Sea region at times of reduced sea ice (Emanuelsson, 2016, 2018; Bertler et al.,

160 2018). Conversely, isotopically-depleted precipitation might occur at times of expanded sea ice, and/or when air masses travel across West Antarctica before reaching RICE. Sea ice in the ERS/Northern AS also influences snow accumulation rate at RICE, so that periods of reduced (increased) SIC are related to increased (reduced) snow accumulation and isotopically-enriched (depleted) water vapor (Emanuelsson et al., 2023).

At RICE and in the wider Ross Sea region, most of the snow accumulation occurs as snowfall, while clear sky precipitation

165 (diamond dust) represents only a minor contributor (Sinclair et al., 2010). Intense snow accumulation episodes typically occur in correspondence to the western flank of blocking anticyclones, when strong meridional (poleward) winds create a corridor drawing isotopically-enriched air masses from the nearby open ocean, north of the sea-ice edge, to RICE (Emanuelsson et al., 2018, 2023). Modern meteorological data highlight that these intense precipitation events related to blocking anticyclones are

responsible for the N-NE winds that prevail at Roosevelt Island. Currently, blocking events occur in a small percentage of time (ca. 12% in the 1979-2014 CE period) but they are responsible for the largest fraction of the annual precipitation at the site (ca. 88%, Emanuelsson et al., 2016). Interestingly, in relation to these large precipitation and extreme surface air temperature events, a “dipole” pattern in temperature, snowfall and sea ice is generated between the ERS and the Western Ross Sea (WRS), and also between the ERS and the Antarctic Peninsula. By interacting with the eastern flank of low-pressure cells centred over the Ross Sea, the blocking anticyclonic events contribute significantly to the antiphase East-West Ross Sea dipole formation (Emanuelsson et al., 2018).

2. Methods

2.1 The RICE ice core

The RICE ice core was drilled on the NE edge of the Ross Ice Shelf, at the summit of Roosevelt Island (79.364°S, 161.706°W, 550 m a.s.l., fig. 1), an ice rise 764 m thick, locally-grounded 214 m below sea level (Bertler et al., 2018; Lee et al., 2020). At RICE, ice accumulates locally, while the floating ice shelf flows around it. In cross section, the RICE surface topography appears quasi-parabolic with flank slopes extending from a blunt peak (Kingslake et al., 2014). The very low horizontal ice flow coupled to local snow accumulation made this site suitable to extract an ice core drilled to bedrock. To date, the main record is estimated to span 83 kyr, providing rich insights of coastal Antarctic climate (Bertler et al., 2018; Winstrup et al., 2019; Lee et al., 2020). In this study, we focus on the top ~300 m of the core, capturing the last 2 ka, where important climate and atmospheric patterns at the site occurred (Bertler et al. 2018). The RICE ice core samples were cut for dust and diatom analyses at the New Zealand ice core facility in Wellington. Each sample consisted in dome-shape ca. 15 cm long slices (15x35 mm) from the side of the RICE main core (cutting plan: <http://www.rice.aq/core-processing.html>).

2.2 Dust analyses

After shipment to Italy, a set of 412 samples spanning the Holocene climate period was measured for dust concentration and grain size at EUROCOLD Laboratory of Milano-Bicocca University. Dust analyses were performed inside a clean room following standard protocols (Delmonte et al., 2017), using Beckman Coulter Multisizers 4 and 4e, both equipped with orifice tubes having an opening of 30 µm. A rigorous intercalibration between the two instruments was implemented prior to the measurements. This setup allows detection of insoluble impurities with equivalent spherical diameter between 600 nm and 18 µm. Within this interval, from the dust size distribution spectra that are defined over 400 channels (log scale), the size distribution indexes of fine particles percent (FPP%) and coarse particle percent (CPP%) were calculated (Delmonte et al. 2017, 2020). Dust mass was calculated from volume-size distribution spectra assuming an average mineral density of 2.5 g/cm³ (Delmonte et al., 2020).

2.3 Diatom analyses

After completion of the dust analyses, residual meltwater aliquots of 10 mL each were filtered on polycarbonate track-etched Isopore™ membranes with a porosity of 0.22 µm. These were mounted on glass slides and observed through a reflected light optical microscope (Olympus BX51M, magnification 100x, 500x, 1000x) in search for diatom valves and fragments. Each valve was identified and counted, then photographed (1000x) and measured for its apical and transapical axis length using the *OLYMPUS Stream Essentials* software. We note that the optical microscope-based approach used in this study is different from former literature works (Tetzner et al., 2022a, 2022b) where scanning electron microscopy (SEM) imaging was used for diatom counting and identification. Thus, in order to estimate the potential counting errors, we compared both methods using a set of 10 samples selected from different depths along the core (from 48 to 625 m depth).

3. Results

The stable water isotope and snow accumulation record from RICE (from Bertler et al., 2018) are reported in figure 2a and 2b, respectively, along with the mineral dust size (fig. 2c) and concentration profile (fig. 2d). This latter shows a pronounced variability (CV ~75% on average) during the last 2 ka, with a mean of about 16-17 ppb (i.e. ng_{dust}/g_{ice}) that is in line with the Holocene average of 15.6 ppb for the site (this study, not shown). For particles smaller than 5 µm in diameter, concentrations are lower than 30 ppb for 90% of the time over the last 2 ka. Given an average snow accumulation rate at RICE (Bertler et al., 2018) of about 25.5 cm w.eq. per year (fig. 2b, data from Winstrup et al., 2019), the average dust flux for particles smaller than about 5 µm can be estimated around $4.2 \pm 3.8 \text{ mg m}^{-2} \text{ yr}^{-1}$ (fig. SF1). This estimate is in line with the flux of ca. $4 \text{ mg m}^{-2} \text{ yr}^{-1}$ calculated for the WAIS ice core site over the last 2.4 ka (Koffman et al., 2014, fig. SF1). Such fluxes are about a factor ~2-3 higher than those calculated for peripheral Antarctic high-elevation sites (e.g. Talos Dome and EPICA-DML). Also, they exceed by a factor ~20 the Holocene dust fluxes calculated for inner East Antarctic plateau sites such as Vostok, Dome C and Dome B (Delmonte et al., 2020). Dust size data from RICE also show a degree of particle sorting that is different from central East Antarctic plateau sites (fig. SF2). Indeed, the FPP% and CPP% parameters span a much broader range interval at RICE (20-80% and 10-50% respectively) with respect to plateau sites (30-55% and 10-30%, respectively fig. SF2).

The decadal-smoothed profiles of dust size and concentration over the last 2 ka are reported in fig. 2 c and d, along with the long-term Loess smoothing to appreciate long-term variability of the records. Dust concentration is expressed in log-scale, as recommended (Petit & Delmonte, 2009; Bouchet, 2024) in order to appreciate the variability of dust background. Overall, there is no correlation between snow accumulation (fig. 2b) and particle concentration (fig. 2d), neither for particles smaller than 10 µm (SF3 a) nor for those below 5 µm (SF3 b). There is also lack of correlation between snow accumulation and dust grain size (SF3 c). Conversely, good agreement exists between dust concentration/flux and dust grain size (SF3 d,

235 e) as confirmed by the Pearson Product Moment Correlation between the variables (supplementary information). This means that the major dust inputs are related to fine particle advection.

Both the dust size and concentration records highlight a long-standing period of relatively high dust input starting around 550-600 CE and ending around 1470-1500 CE (fig. 2 d). The beginning and the end of this period broadly coincide with the two-step changes of δD (fig. 2 a), identified at $580 \text{ CE} \pm 27 \text{ years}$ and $1477 \text{ CE} \pm 10 \text{ years}$ by Bertler et al. (2018) using a

240 minimum threshold parameterisation to achieve a minimised residual error. We note however that a detailed comparison between dust and stable isotope records in terms of leads and lags of changes is limited by the very different sampling resolution of the two records. In correspondence to the period from about 550 CE to about 1470 CE, when the stable water isotope record shows an increase of 3‰, the dust record shows concentrations (and fluxes) higher than average for more than 50% of time, while during the following period from 1470 CE to about 1900 CE, when the stable isotope increases again of

245 5‰, the dust levels sharply drop to relatively low levels, remaining below average for about 88% of time. The relative difference of dust concentration and fluxes between the two periods 0-550 CE, 550-1500 CE and 1500-1900 CE can be better appreciated from boxplot graphs (SF4). These two latter periods, that are of particular interest to this study, proved to have statistically-significant differences in dust concentration and fluxes on the basis of t-test statistics (SF4).

250 The stratigraphic record of aeolian diatoms from the RICE ice core is shown in fig. 2e and fig. SF5 (b to e). Both the absolute valve and the valve fragment abundance from this study were normalized considering the time period represented by each sample, spanning ~ 0.6 to ~ 2.5 years, in agreement with former studies (Tetzner et al., 2021). The diatom record shows a background influx in the order of 180 valves per Liter per year ($\text{valves L}^{-1} \text{ yr}^{-1}$) before about 1500 CE, with two minor increases of up to about 2000 valves $\text{L}^{-1} \text{ yr}^{-1}$ around 1200 CE. After the ~ 1470 CE event of drastic dust decrease and increase in the

255 stable water isotope values, two prominent diatom peaks appear. These peaks exceed 4000 valves $\text{L}^{-1} \text{ yr}^{-1}$ and are unprecedented over the last 2 ka (fig. 2e, 6b, SF5) and even over the Holocene (not shown). Diatom peaks are particularly prominent in the periods 1530-1610 CE and 1700-1830 CE for all three indicators - absolute diatom concentration, diatom flux and number of valve fragments detected in the samples (fig. SF5). As diatom concentration and flux data are not lognormally-distributed, the nonparametric Mann-Whitney Rank Sum Test was used as statistic tool to compare the total valve concentration and flux

260 between 1500-1900 CE and the earlier period (0-1500 CE). Results confirm that the difference in the median values between the two groups is greater than would be expected by chance, i.e. there is a statistically significant difference between the two periods.

We note that the optical-based procedure adopted in this study for diatom counting can be considered as reliable as the SEM analysis: indeed, over a total of 184 valves and 84 fragments, only 2 valves and 16 fragments were not found when using the

265 optical method (SF. We estimate therefore that the absolute optical-based diatom abundances reported in this work could represent an underestimate of about $\sim 1\%$ and $\sim 19\%$ the SEM-based analysis. The relatively higher percentage obtained for fragments could be explained by their comparatively smaller size, making them more difficult to identify.

While entire valves could be identified to the species level, this was not the case for most diatom fragments. More than 98.5% of diatom valves were *Fragilariopsis* spp. (fig 3), which we consider as a unique group. In particular, we observed *F. nana* and *F. cylindrus*, with occasional presence of *F. curta* (fig. 3). Sporadically, doublets of two *F. cylindrus* valves were detected (fig. 3d), in particular in the most recent section of the record (fig 2e). Results from morphometric measurements of entire valves oriented in valve view on the filters (fig. 4) show that about 95% of valves display apical axis between 3.4 and 11 μm (mode $\sim 5.3 \mu\text{m}$) and transapical axis between 1 and 3.5 μm (mode $\sim 2.2 \mu\text{m}$). Thus, most diatoms are small-sized, with dimensions similar to those of *F. nana* and *F. cylindrus*, i.e. similar to the size of mineral dust at RICE (Winton et al., 2016b). This characteristics prevents the use of filtration techniques to separate dust and diatoms, or the use of deep neural networks for the identification of diatoms within the samples themselves (Maffezzoli et al., 2023).

4. Discussion

4.1 Transport of dust and diatoms to RICE

The influx of mineral dust aerosols onto the Antarctic ice sheet exhibits significant spatial and altitudinal variation, as highlighted by the pronounced dust flux gradients observed in both East and West Antarctica (SF1). While the central East Antarctic plateau regions are exclusively impacted by well-sorted dust of remote origin, as evidenced by the very low flux values and the small size of the dust grains, West Antarctica (Koffman et al., 2014) and sites at the periphery of the Antarctic ice sheet (Delmonte et al., 2013; Bory et al., 2010) experience a mixture of local and remote dust sources, as well as a different atmospheric transport regime compared to plateau sites (Petit & Delmonte, 2009). In this respect, our new dust data from RICE offer an important addition to the understanding of the dust cycle in coastal, low-elevation sites. Indeed, the paleoclimatic significance of aeolian dust and diatoms transported to RICE is closely related to its geographic and glaciological setting.

Roosevelt Island is a grounded coastal ice rise at the northeastern margin of the Ross Ice Shelf, deeply influenced by its proximity to the open ocean and its neighbouring sea ice zone. Hence, the transport of terrestrial and marine aerosols to the site is very complex. Back trajectory analyses (5 days) of seasonal airmasses for the period 2006-2012 CE (Tuohy et al., 2015) revealed that austral summer trajectories are dominated by three clusters. The first is characterized by a local short-range transport, while the two additional clusters represent long-range transport. One of these long-range transport clusters comprises the distal oceanic component driven by low-pressure systems that move over the Southern Ocean. This long-range cluster has been shown to be responsible for the advection of marine aerosols to the RICE site (Tuohy et al. 2015). The second long-range cluster includes trajectories of air masses that travel over long distances, across the South Pacific landmasses and then reach the RICE site via the West Antarctic/Amundsen-Bellingshausen Seas (ABS, Tuohy et al., 2015). These latter pathways are associated with the most significant transport of heavy metals to RICE and therefore modulate the long-range transport of

mineral dust, that is thus sensitive to large-scale atmospheric circulation patterns in the South Pacific sector of the Southern Ocean (Tuohy et al., 2015). Among atmospheric forcing factors responsible for the modulation of long-range transport of dust, we mention the state of the Amundsen Sea Low (ASL), a climatological low pressure centre in the ABS and Eastern Ross Sea area, which is in turn strongly affected by large-scale atmospheric circulation modes of variability such as the Southern Annular Mode (SAM) and the El Niño-Southern Oscillation (ENSO, Emanuelsson et al., 2023).

The aeolian transport of diatoms at RICE follows instead a different atmospheric pattern. Most diatom species are marine planktonic and sea ice-related, supporting a proximal marine origin of diatom-transporting air masses. This hypothesis is corroborated by the evidence of an exceptionally high degree of valve preservation, sometimes being present as doublets in our record. These fresh-looking aspect of diatoms suggest a rapid transport of the cells directly from the proximal marine source to the RICE ice core site, and support the hypothesis that the main diatom source at the site is represented by the nearby Ross Sea waters.

Former studies on West Antarctica and the Antarctic Peninsula (Allen et al., 2020, Tetzner et al., 2021, 2022a, 2022b) demonstrated that diatom species and their seasonal variability vary between coastal low elevation sites and continental, high elevation sites of the Antarctic Peninsula. While the former display a marked seasonal signal dominated by species like *F. cylindrus* and *F. curta*, typically sourced from the seasonal sea ice zone (SSIZ), the latter display a higher proportion of open ocean diatoms, distally-sourced and lacking a clear seasonality. In this sense, RICE mostly resembles coastal sites of the Peninsula, where local diatom transport is predominantly related to local oceanic air mass transport. The stratigraphic records of aeolian dust and diatoms at RICE, therefore, are highly complementary since they are related to different types of atmospheric transport; as discussed below, these new records open new perspectives on the interpretation of the paleoclimatic signals from the core.

4.2 Environmental changes at RICE in the context of the Ross Sea region: the first part of the record

The reconstruction of dust and diatom variability at RICE offers a valuable opportunity to explore the influence of key drivers of regional climate conditions over the past two millennia, as well as the major environmental changes in the Ross Sea area. Throughout the record, we observe that periods of elevated dust concentration and flux are generally associated with finer particles. This suggests that the most significant dust transport events at RICE are linked to the advection of remotely sourced particles, rather than local transport. Although no statistically significant relationship is found at finer time scales, periods of increased dust input at RICE, including the extended period from 550-1470 CE, which encompasses the Medieval Climate Anomaly (MCA), appear to coincide with higher snow accumulation rates and more enriched stable water isotope values, at least until around 1250-1300 CE. According to Bertler et al. (2018) stable isotopes show a statistically-significant, negative correlation with sea-ice extent in the South Pacific (AS/ERS). Thus, periods of increased dust input correspond broadly to periods of reduced sea-ice extent in the ERS sector of the Southern Ocean as suggested by the increased snow accumulation rate and by more enriched stable water isotopes. This could be interpreted as a more effective penetration of long-range

northerly air masses to the RICE site, that occurred in relation to the atmospheric circulation regime. Additional evidence is provided by the diatom records. Dust-rich air masses typically travel above the marine boundary layer (Petit & Delmonte, 2009). Consequently, we do not expect to observe significant input of open ocean marine diatoms together with mineral dust. In fact, our data indicate that during periods of increased dust content, only background levels of aeolian diatom influx are detected at the site. (fig. 2, fig. SF5).

To put our climate reconstruction at RICE into the broader context of the Ross Sea region, we compare our data with TALDICE ice core records from Talos Dome. This site is located on the periphery of the East Antarctic plateau facing the Ross Sea and the South Pacific (fig.1). The sea-salt sodium (ssNa) record from the site has been interpreted as related to the extent of pack ice newly-formed in the Western part of the Ross Sea. We observe therefore (fig. 5b) that around 800-1000 CE the extent of pack-ice neoformation in the WRS was very low (Mezgec et al., 2017), while it increased from ~1000 CE to 1300 CE. In parallel, we observe that between ~800 and 1000 CE, the Ross Sea “polynya efficiency” index was indeed also quite low, while it increased from about 1000 CE. This parameter, introduced by Mezgec et al. (2017), is linked to the activity of the Ross Sea polynya, particularly on its westernmost side. It is derived from a stacked marine record of *F. curta* from the coastal sea ice of the WRS, along with the ssNa record from Taylor Dome.

Around 1300 CE, the RICE snow accumulation reaches its maximum (ERS sea ice minimum), while dust influx remains high. Therefore, we deduce that 1300 CE is the time when the sea ice dipole into the Ross Sea reaches its maximum expression, with maximum pack-ice extent in the WRS and minimum sea ice in the ERS and Amundsen Sea (fig. 5 b-c). At this time, the dust influx to RICE steadily remained at high levels (fig. 5a), suggesting an efficient marine air mass penetration to the site.

4.2.1. The dipole pattern and climate drivers

To accurately interpret our 2 kyr record, it is crucial to consider current meteorological patterns in the Ross Sea as well as the meteorological effects of El Niño and La Niña. The establishment of a “dipole-like” pattern in air temperature and sea-ice concentrations between the ERS and WRS is often associated with formation of near-stationary anticyclones (Emanuelsson, 2018). These impede the progression of the westerly circulation and induce a significant meridional transport to RICE from N-NE (Turner et al. 2016), that is responsible for humidity advection to the site. Indeed, several research studies highlight the importance of the Amundsen Sea Low (ASL) in strongly influencing the climate of the Amundsen–Bellingshausen Sea (ABS)/ERS region, and hence the climate at Roosevelt Island. The ASL is an area of climatologically low atmospheric pressure characterized by a large geopotential height variability, associated with both depressions and blocking high pressure ridges. When these near-stationary anticyclones form, they impede the progression of the westerly circulation and associated storm tracks. It has been observed (Turner et al., 2013; O’Connor et al., 2021; Rahpael et al., 2019; You and Maycock, 2019) that the ASL depth and location, both latitude and longitude, vary in relation to other climate drivers, including El Niño Southern Oscillation (ENSO), Pacific Decadal Oscillation (PDO) and the Southern Annular Mode (SAM). In particular, the frequency

370 of blocking events in the southern high latitudes increases significantly during ENSO warm phases (El Niño), particularly over
the southeast Pacific during the austral spring and summer (Renwick, 1998). Observational data provide evidence that both
central Pacific (CP) and eastern Pacific (EP) El Niño climate conditions induce anomalous northerly wind flow along the
western side of the blocking ridge in the Amundsen/ERS. This favours poleward movement of sea ice and net sea ice loss
375 forcing in the Ross Sea is double-sided: while the eastern part of the Ross Sea displays a statistically-significant negative
correlation between the Southern Oscillation Index (SOI) and temperature, with warmer temperatures during El Niño events,
the coastal Antarctic areas of Victoria Land show positive or non-significant correlation with SOI, with generally colder
temperatures during El Niño events, increased sea ice, southerly winds, surface temperature cooling and lengthening of the
sea-ice season (Li et al., 2021). The reason for the tight coupling between El Niño and atmospheric circulation in the area of
380 RICE and more generally in the Ross Sea (Bertler et al. 2004) relies on changes of the split jet in the proximity of New Zealand.
This induces a subsequent weakening of the polar front jet during El Niño, an eastward shift and weakening of ASL, reduced
cyclone density in the ERS and more frequent blocking, with associated thermal and mechanical forcing (Bertler et al. 2011).
According to the review study of Li et al. (2021), sea ice decreases by 10-20% in the Amundsen and ERS during El Niño
events, but increases in the Eastern Amundsen and Bellingshausen Sea and in the Weddell Sea. This pattern is known as the
385 Antarctic sea ice dipole, representing the leading mode of ENSO- related Antarctic Sea ice variability.

On longer (climatological) timescales, these considerations suggest a possible relationship between dust input to RICE, snow
accumulation at the site, stable water isotopes ratios, sea ice area, and ENSO. Interestingly, the precipitation-based Southern
Oscillation Index (SOI_{pr}) reconstruction (Yan et al., 2011) for the last 2000 years (fig. 5d), along with the Galapagos rainfall
390 history (fig. 5d) derived from El Junco lake level reconstruction (Conroy et al., 2008) display a maximum of El Niño-like
conditions around 1300 CE (ca. 1000-1400 CE). Also, the laminated sedimentation record from Laguna Pallcacocha in
southern Ecuador (fig. 5e), which is sought to capture ENSO variability during the Holocene, exhibits increased El Niño-like
conditions between 1000 and 1400 CE (Moy et al., 2002). This time period coincides with maximum expression of the Ross
Sea dipole as expressed by the comparison of stable water isotope records of RICE and TALDICE (Bertler et al., 2018) and
395 imprinted in the ssNa record from TALDICE.

Our observations are coherent with conclusions from Koffman et al. (2014), who observed a southern shift of Southern
Westerly Winds (SWW) and increased meridional dust transport to WAIS divide at times of El Niño. We infer that this can
be due to the blocking events associated with enhanced air mass advection to RICE from N-NE: by impeding zonal westerly
winds in the 45°–70°S, 90°–150°W region (Emanuelsson, 2018) and diverting the SWW flow towards West Antarctica, this
400 effect has probably lead to an enhanced meridional flow to WAIS divide.

Similarly, the SWW shift southwards in association with El Niño is also imprinted in the marine sediment record GeoB3313-
1 from the Chilean continental slope (41°S), as already noted by Koffman et al. (2014). This indicates enhanced aridity around
1110–1395 CE (fig 5f) in Southern Chile, a feature that is also notable around 300 CE. Indeed, it is worth noting that around

300-400 CE similar El Niño-like conditions are observed, with high dust influx at RICE and reduced sea ice extent in the ERS. This is accompanied by enhanced Ross Sea polynya activity and increased coarse particle transport at WAIS Divide (Koffman et al., 2014), supporting the possible relationship observed in the most recent part of the record. We note however that in the case of this possible El Niño “analogue” there is a lack of response in the RICE stable isotope record, which does not show the typical increase expected (fig. 1a). This is likely because 300 CE marks a period of dynamic changes in the Ross Ice Shelf, with the calving line either terminating or having just completed its last phase of retreat. Under these conditions, it can be hypothesized that the surface waters of the Eastern Ross Sea were much cooler, leading to a different response in stable isotopes. Consequently, we leave the interpretation of this potential analogue as an open question for future research.

4.3 The period 1470-1900 CE

After about 1470 CE, the RICE record is characterized by a sudden drop in dust concentration and flux, accompanied by a more gradual snow accumulation decrease suggesting increased pack ice in the ERS/Amundsen Sea. In parallel, the stable water isotope composition at RICE increases abruptly, in apparent contradiction to the general relationship between snow accumulation/sea ice and stable water isotopes observed in the earlier part of the record. Bertler et al. (2018) hypothesized that a novel source for isotopically-enriched vapor could justify this sudden stable water isotope increase. Interestingly, such isotope enrichment during the LIA time frame coincides with the appearance of unprecedented peaks in the concentration of sea ice-related and marine planktonic diatoms (fig. 2, 6, S4). These are predominantly observed between ~1500 CE and 1850 CE as two separate peaks around 1530-1610 CE and 1700-1830 CE.

Diatom peaks occur concurrently with stable water isotope enrichments and decreased snow accumulation. This means they correspond to a period of intense influence of local low-elevation marine air masses originating from the marine boundary layer, as also suggested by the significant increase of marine compounds (Na^+ , Ca^{2+} , K^+ , Mg^{2+} , SO_4^{2-}) in the RICE ice core (fig. 6, from Brightley, 2017). Comparable values of aeolian diatom fluxes have never been observed along the RICE record and point towards the presence of newly-exposed oceanic water masses in proximity of the site. We note that the position of the calving line remained almost the same during that period (Yokoyama et al., 2016); therefore, we believe the diatom peaks can be related to a new phase of expansion of the Ross Sea polynya. In particular, we suggest an enlargement of the Ross Sea polynya along the central and eastern portion of the Ross Ice Shelf front, possibly implying the opening of the so called *Roosevelt Island Polynya*, intended as the eastward protrusion of the much larger Ross Sea polynya. This could have had an important influence at a regional scale.

4.3.1 Ross Sea polynya formation and associated meteorological patterns

Diatoms windblown to the RICE site likely underwent a very short transport directly from the adjacent sea, as revealed mainly by their excellent degree of preservation. Specimens consist almost exclusively of marine planktonic and sea ice-related

species, that we believe to be entrained by winds during the early austral spring, at the time of the rapid increase of the polynya areal extent. The Ross Sea Polynya is considered to be primarily a wind-driven polynya (Zwally et al., 1985) although it may be in part thermally-driven (Jacobs and Comiso, 1989). The enlargement of the polynya, mostly occurring west of the date line, is mainly related to enhanced katabatic air flow descending from the Siple Coast of West Antarctica, and to barrier winds flowing northward along the Transantarctic Mountains (Bromwich et al., 1998, Morales Maqueda et al., 2004). Ice production and drift from the Antarctic Ross Sea polynya is also modulated by a semipermanent low-pressure system located to the east (Bromwich et al., 1998; Drucker et al., 2011). In the Ross Sea, in particular, this low-pressure system produces strong southerly winds off the western Ross Ice Shelf and a return air flow towards Roosevelt Island (Drucker et al., 2011). This return flow is particularly relevant as the potential driver for the atmospheric transport of diatom and marine aerosol to the RICE site from the nearby sea surface waters.

The Holocene history of the Ross Sea polynya activity documented by Mezgec et al. (2017) is mainly based on marine sediment and ice core data from the WRS and from East Antarctica. Thus, it represents a comprehensive picture of the W-NW Ross Sea polynya, where the major enlargement typically occurs, but it is not possible to exclude that the development of the polynya in the central part of the ice shelf front and towards the much smaller Roosevelt Island polynya might have had a slightly different evolution. Present-day data (Wang et al., 2022; Tianjiao et al., 2022) highlight that the eastward expansion of the polynya is generally correlated to the integrated areal expansion of the polynya itself. This evidence could account for the agreement between the diatom peaks in the RICE records during the LIA and the increase in the “polynya efficiency” index (Mezgec et al., 2017). Bromwich et al. (1993) observed that the speed of katabatic surges from the Siple Coast plays a key role in modulating the opening of the polynya in the central part of the Ross Ice Shelf front. It is therefore plausible that the intensity of katabatic surges from the Siple Coast increased during the Little Ice Age (LIA), contributing to a significant expansion of the polynya along the central and eastern parts of the Ross Ice Shelf front. In the context of the present-day climate, enhanced southerly winds off the central Ross Ice Shelf are likely associated with a deeper low-pressure system centered approximately north of RICE. Therefore, this cyclonic circulation system may drive the advection of marine aerosol-rich air masses towards our drilling site.

Meteorological observations highlight that katabatic surges typically promote the establishment and development of mesoscale cyclones inside the Ross Sea. After their formation, they then move northeastwards, ultimately bringing maritime air masses to the site (Carrasco et al., 2003). Numerical simulations by Heinemann and Klein (2003) show that the topography of Antarctica plays an essential role in mesocyclone formation where the convergence of katabatic airflow provides cyclonic shear for the initial formation of the cyclone. Therefore, while katabatic winds represent the principal factor leading to the primary opening and development of coastal polynyas, it is also true that these latter, in turn, provide an area of open water near the coast acting as a source for sensible and latent heat fluxes promoting low-level baroclinicity between the open water and the continent thus allowing further warming and moistening of the atmosphere over the polynya and contributing to further mesocyclogenesis (Klein and Heinemann, 2001).

We conclude that there is a possibility of a positive feedback mechanism between katabatic winds, polynya formation and development of mesoscale cyclones. After its initial development, then the subsequent evolution of mesocyclones requires upper-level synoptic-scale support to generate a synoptic or sub-synoptic system (Heinemann and Klein, 2003, Carrasco et al., 2003).

475

4.3.2 Atmospheric conditions leading to enhanced diatom transport during the LIA

Given the above-mentioned meteorological evidence for present-day climate, we hypothesize that during the LIA the local maritime air mass advection towards the RICE site, responsible for diatom and marine aerosol transport to the site, might have
480 been related to increased katabatic winds over the central and Western part of the Ross Ice Shelf with maximum polynya development and enhanced atmospheric return flow of local maritime air masses to RICE (fig. 6 c). We believe that these maritime, diatom-rich air masses derive from low-elevation atmospheric layers. In fact, the dynamical and thermodynamical interactions between atmosphere and ocean are strongly influenced by the presence of the polynya, that modifies the vertical structure of the atmosphere promoting the development of a relatively thicker and well-mixed convective boundary layer
485 (Fusco et al., 2009). We also note that the opening of the Roosevelt Island polynya had influence on local scale, since the sodium record from Siple Dome, located some hundreds of kilometres on the Siple Coast of West Antarctica (Kreutz et al., 1997) mimics the expansion of the whole Ross Sea polynya (fig. 6 a). The hypothesis of a significant enlargement of the RS polynya during the LIA is also supported by data from the western side of the Ross Sea, pointing towards prolonged cold climate conditions with significant increase of katabatic winds and polynya areal extent between the 16th century and the
490 beginning of the 19th century. The TALDICE ice core shows the most negative stable water isotope values of the last 2000 years (Stenni et al., 2011) and an 11% decrease in snow accumulation compared to the preceding period, indicating colder and windier conditions at that time. Indeed, cooling in East Antarctic and the Ross Sea could lead to stronger katabatic flow, in turn leading to an increased polynya efficiency and more sea-ice production (Mezgec et al. 2017). The Taylor Dome record shows prolonged cold stable water isotope temperature anomalies (Steig et al., 2000), while the stable water isotope and
495 geochemical records from Mt. Erebus Saddle (Rhodes et al., 2012) highlight that the region experienced colder than average temperatures prior to 1850 CE and strong katabatic winds between 1500 and 1800 AD. According to Rhodes et al. (2012), prior to 1875 CE the biological productivity in the Ross Sea polynya was ~80% higher than any subsequent time. Bertler et al. (2011) also report colder temperatures and more extensive sea ice, as well as decreased snow accumulation in the WRS at the time of the LIA. The increased efficiency of the RS polynya over the last ~500-600 years is also testified by important
500 ecological variations in Victoria Land (figure 6); indeed, during this period, Hall et al. (2006, 2023) observe the almost complete disappearance of elephant seal (*Mirounga leonina*) colonies in Victoria Land, related to the increased persistence of coastal sea ice. A key factor for the reproductive success of elephant seals is the proximity of open water to the nursery sites. Thus, the complete disappearance of elephant seal colonies in Victoria Land during the LIA is interpreted be related by a significant increase of coastal sea ice. This hypothesis is also corroborated by independent marine data as those from Edisto

505 inlet, in the North-Western Ross Sea (Tesi et al., 2020), where persistent summer fast ice was observed over the last 700 years. Since the formation, maintenance and variability of Antarctic polynyas is known to be influenced by landfast sea ice (Fraser et al., 2019; Mezgec et al., 2017), we conclude that our data confirm the link between the irreversible elephant seal population abandonment of the Victoria Land coast during the LIA and the increased extension and occurrence of the Ross Sea polynya. Between about 1470 CE and 1900 CE, a time for which we infer the expansion and development of the Roosevelt Island
510 polynya, predominance of positive SOI_{pr} and enhanced Pacific Walker circulation (Yan et al., 2011) suggest a more La Niña-like mean state. We note that here we use the recent SOI_{pr} hydrological reconstruction that includes records from the Indo-Pacific, from the central tropical Pacific and from the eastern equatorial Pacific and which is an atmospheric/hydrological record in agreement with other hydrological records (Rein et al., 2005) indicating a more La Niña-like mean state during the LIA. However, this series conflicts with sea surface temperature (SST) reconstructions that suggested the LIA was
515 characterized by a more El Niño-like state, as discussed in detail by Yan et al. (2011). Under La Niña-like conditions, the polar front jet (Turner, 2013) and the ASL became more intense (deeper ASL), while the low-level easterly jet along with the katabatic flow from the Antarctic are enhanced (Bertler et al., 2006). As a result, a deeper ASL often coincides with a larger Ross Sea polynya, as also revealed (Wang et al., 2022) by modern satellite data.

520 **5. Conclusions**

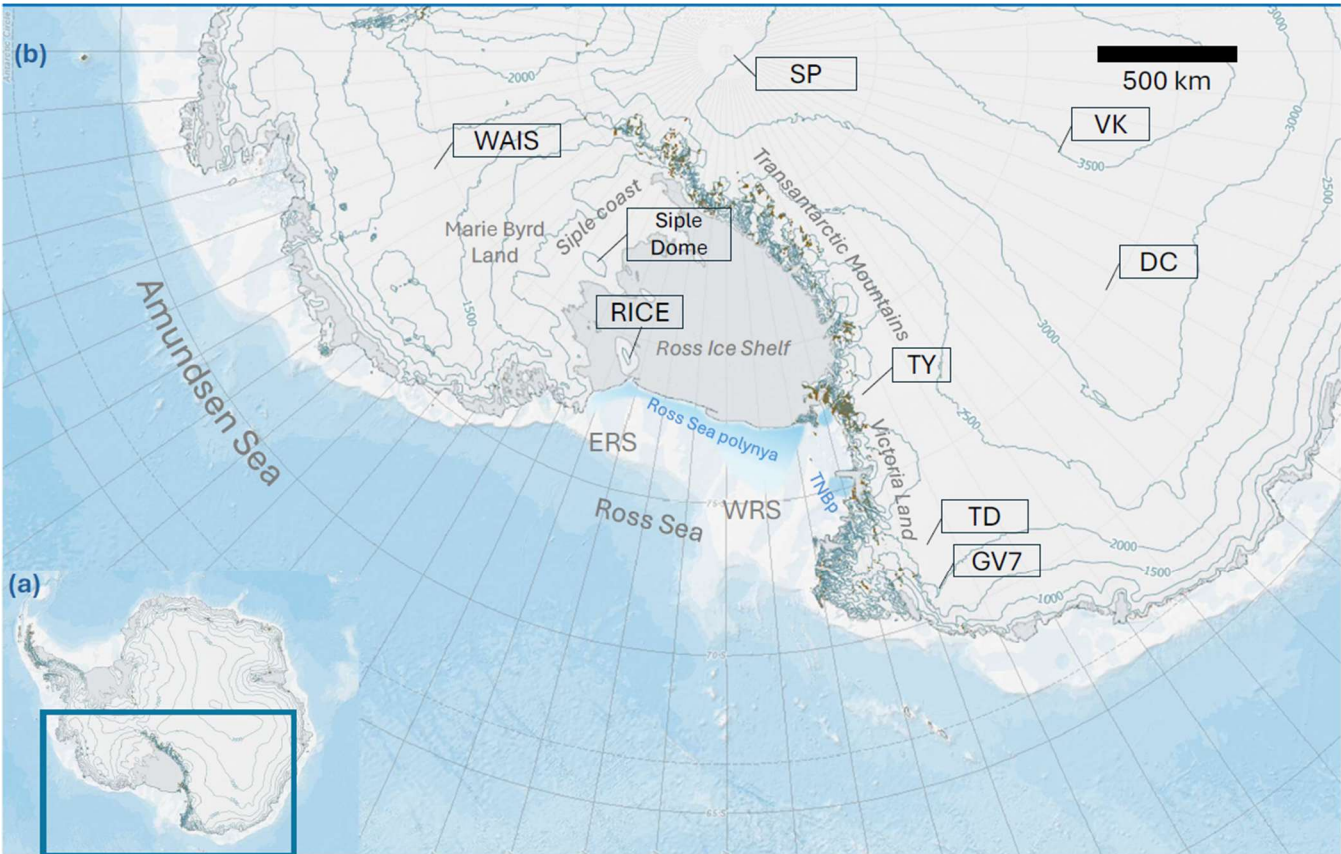
The aeolian dust and diatom influx at RICE are related, respectively, to large-scale atmospheric circulation patterns within the ERS/Amundsen Sea and to local oceanic influence of air masses from the marine boundary layer. The complementarity of
these proxies allows us to appreciate the importance of climatic and atmospheric changes experienced by Roosevelt Island
525 over the last 2 kyr, in response to some major forcing factors such as ENSO.

During the 550-1470 CE period, when higher/less depleted stable water isotope values are observed, the increased importance of blocking ridges in the Amundsen Sea and a weakened ASL promoted dust-rich air mass advection to RICE. This pattern was accompanied by an increasing trend in snow accumulation and reduced sea ice in the ERS/Amundsen Sea. At about 1300
530 CE, the maximum expression of the Ross Sea dipole is reached, with enhanced katabatic outflow in the WRS and reactivation of the Ross Sea polynya. At the same time, the ERS was still under the influence of blocking ridges promoting maritime air mass advection to RICE and southward shift of the South Westerly Winds, in agreement with data from West Antarctica and South America. After 1470 CE, the RICE site was subject to a rapid atmospheric circulation reorganization in response to the development of the Roosevelt Island Polynya, leading to an unprecedented diatom input at RICE and low dust influx, in tandem with decreased snow accumulation and increased sea-ice extent in the ERS/Amundsen Sea. Thus, we suggest that polynya
535 efficiency increases over this period encompassing the LIA is associated with the eastward expansion of the Roosevelt Island polynya, as a protrusion of the much larger Ross Sea polynya, but with an important regional impact in the Ross Sea region. For the RICE site, we suggest that several drivers contribute to the long-term dust, sea-ice and polynya variability, but ENSO-

driven teleconnections are particularly prominent. On a longer (multidecadal) timescale it seems that El Niño-dominating conditions promoted the establishment of the Ross Sea dipole, while La Niña conditions favoured a deeper ASL and an eastward expansion of the polynya.

540

FIGURES AND FIGURE CAPTIONS



545 **Fig. 1-** Map of Antarctica with regions and drilling sites cited in the text (source: SCAR Antarctic Digital Database, <https://add.scar.org/>). ERS: Eastern Ross Sea; WRS: Western Ross Sea; SP: South Pole; DC: Dome C; VK: Vostok; TY: Taylor Dome; TD: Talos Dome. The light blue shaded area (redrawn from Mezgec et al., 2017) represent the Ross Sea polynya, and the much smaller McMurdo Sound and Terra Nova Bay (TNBp) polynyas.

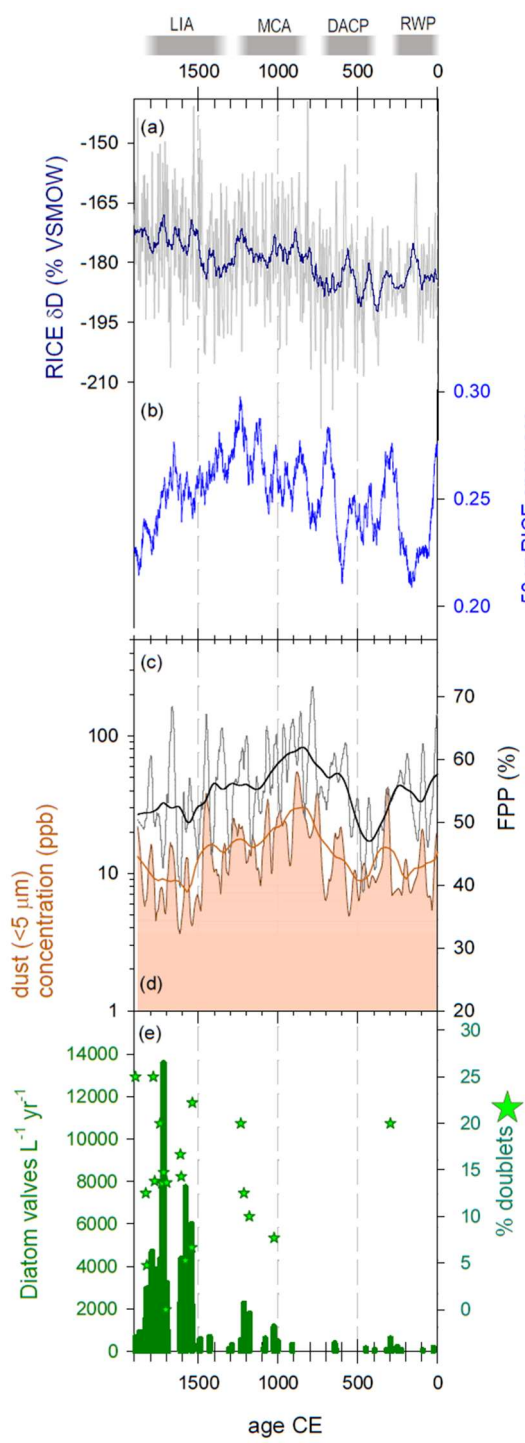


Fig. 2- The climate history of RICE over the past ~2000 years. RWP: Roman Warm Period; DACP: Dark Ages Cold Period; MCA: Medieval Climate Anomaly; LIA: Little Ice Age.

(a) RICE water stable isotope record (δD ‰VSMOW; blue line: 50- yrs running mean);

(b) Snow accumulation at the site (50- yrs running mean). (a) and (b) data from Bertler et al., 2018.

(c) Dust size index FPP (%) defined as in Delmonte et al. (2017), 20- yrs running mean and Loess local smoothing (polynomial degree 1, sampling proportion 0.1);

(d) Concentration (log) of dust particles smaller than 5 μm, 20- yrs running mean and Loess local smoothing as in (c);

(e) Diatom content of samples, expressed as number of diatom valves per Liter per year. Green stars indicate the percentage of doublets in the samples.

Plots (c), (d) and (e) are generated from data obtained in this work; these are reported in Supplementary Tables ST1 and ST2.

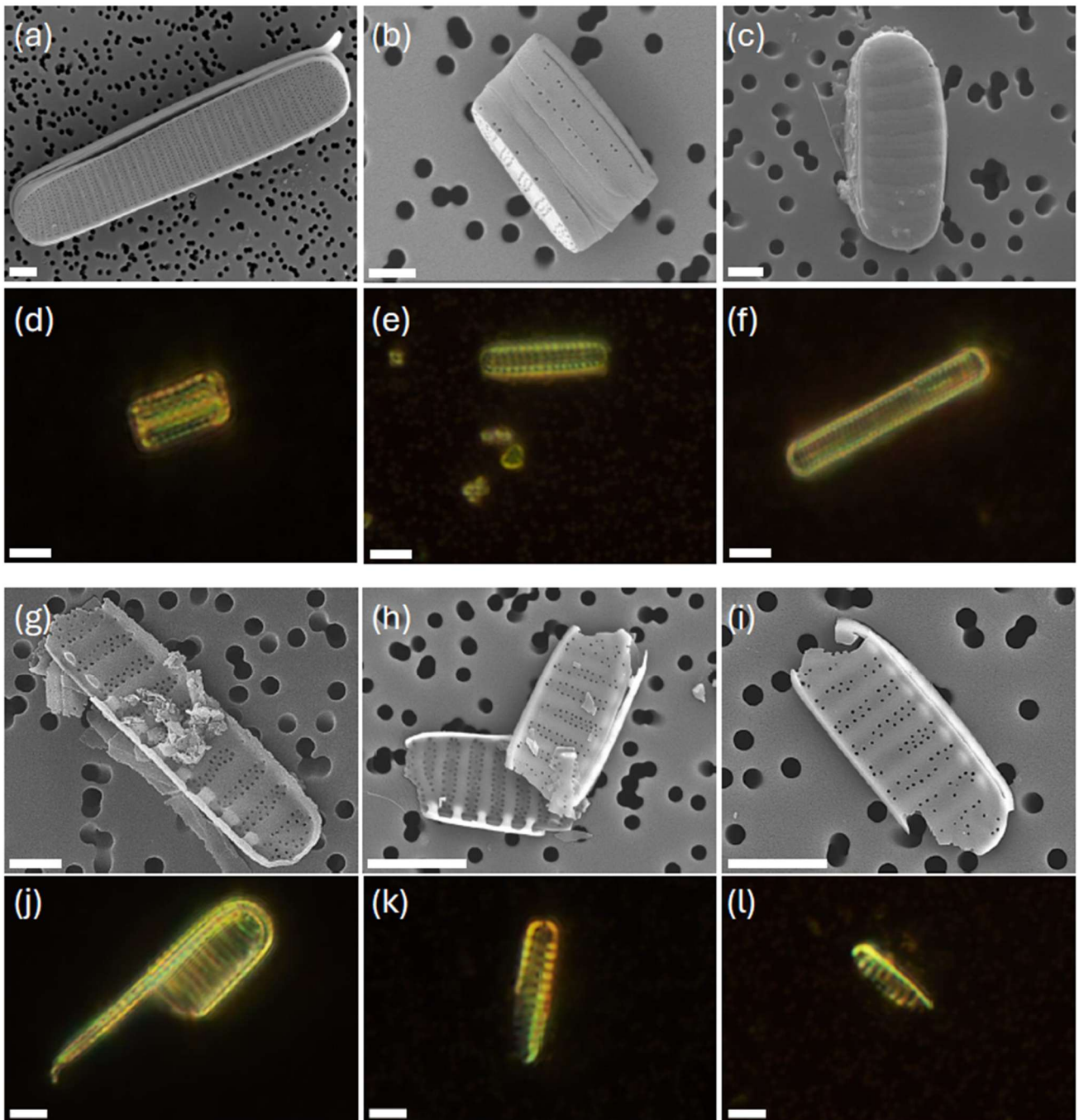
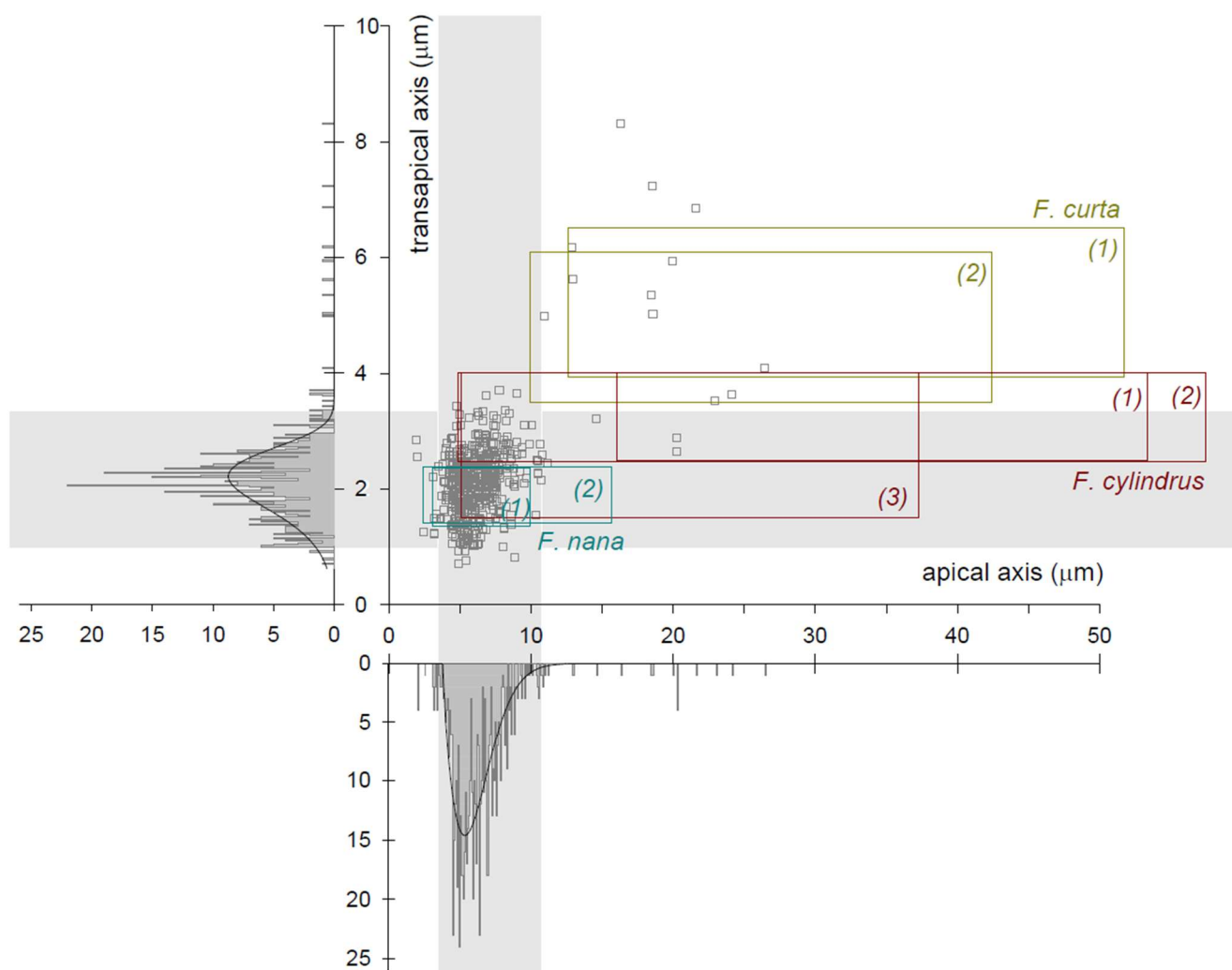


Fig. 3- Scanning Electron Microscope (a, b, c, g, h, i) and optical microscope (d, e, f, j, k, l) images of entire diatom valves (a to f) and valve fragments (g to l). Scale bar: 1 μm for SEM images and 5 μm for optical images (magnification 1000x).



575

Fig. 4- Morphometric data of entire valves from the RICE ice core. Apical axis (μm) vs transapical axis (μm). Frequency histograms (bottom and left) are also reported. Grey bands indicate the interval where 95% of specimens are included. Boxes with n.1 refer to morphometric data for *F.cylindrus*, *F.nana*, *F.curta* from Cefarelli et al., 2010; boxes marked with n.2 refer to earlier literature morphometric data collected and listed in Cefarelli et al., 2010. Box with n. 3 refers to data from Lundholm and Hasle (2008) for *F.cylindrus*.

580

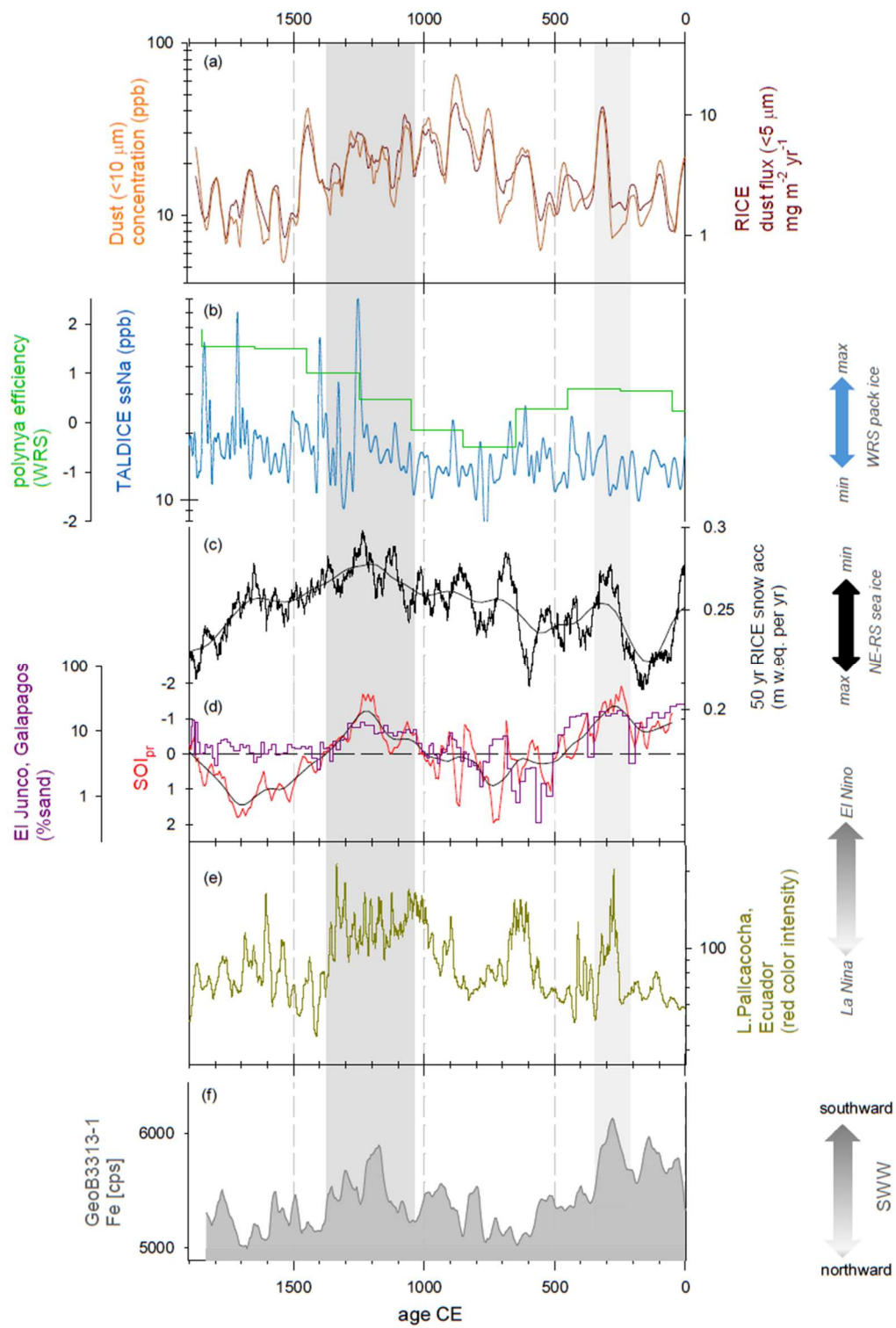
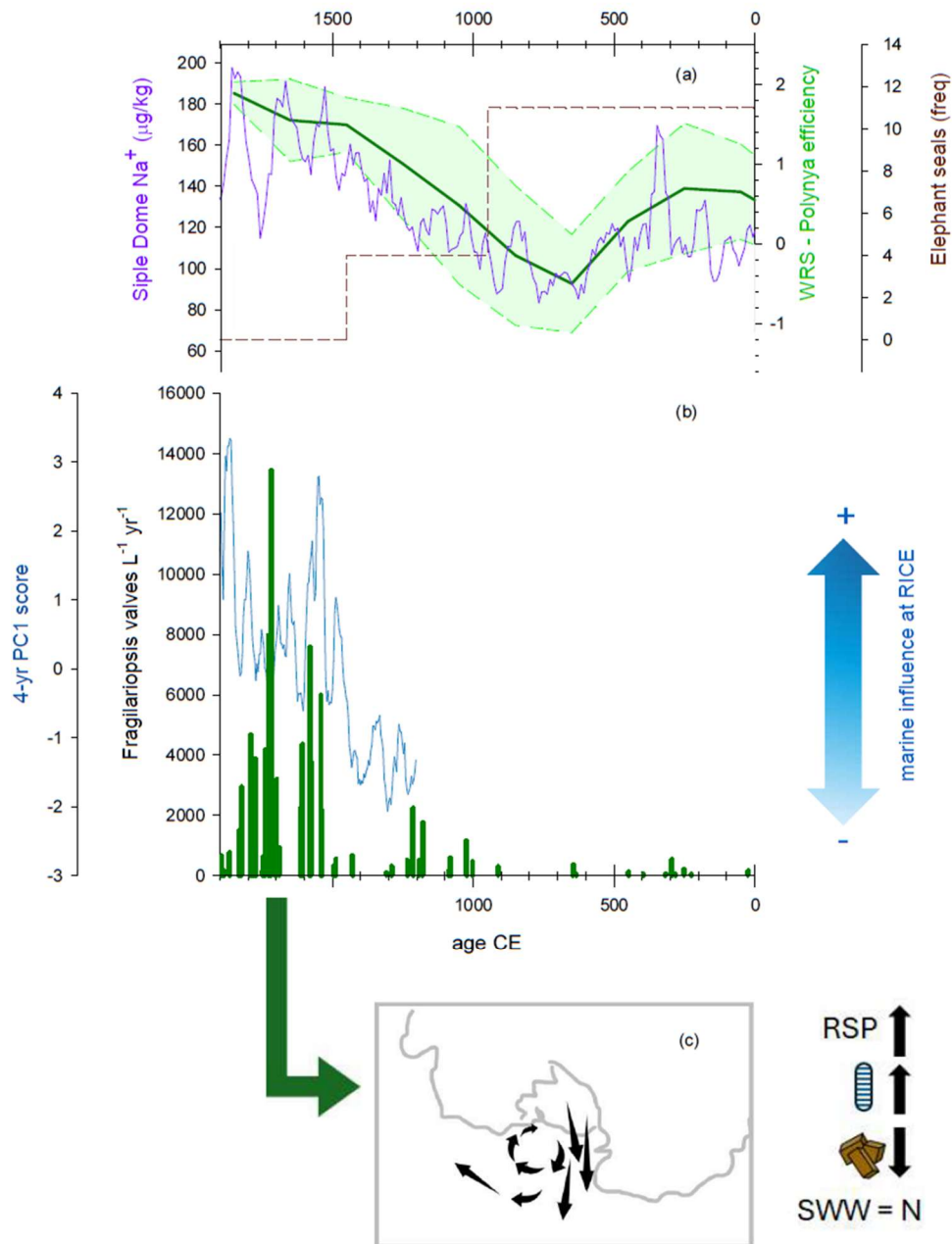


Fig. 5- Comparison of ice core and climate records from the Southern Hemisphere over the last 2000 years. (a) Concentration of dust particles smaller than 10 μm (ppb), and flux ($\text{mg m}^{-2} \text{ year}^{-1}$) of particles smaller than 5 μm . (b) Sea salt Sodium (ssNa) concentration at TALDICE and polynya efficiency (Mezgec et al., 2017). (c) RICE snow accumulation rate, as in fig. 2b. (d) Red line: Southern Oscillation Index (SOI_{pr}) record (with Loess smooth superposed, black line) from Yan et al., 2011. This index was calculated as the difference between the reconstructed precipitation records from Indonesia and the Galapagos. Purple line: rainfall history of the Galapagos, used in the reconstruction of SOI_{pr} , but extending on a longer time period. This series is derived from a lake level reconstruction based on grain size data from Lago El Junco sediment core. (e) Laguna Pallcacocha, Ecuador red color intensity record of sediments from Moy et al., 2022. El Niño-related high precipitation events are related to greater color intensities. (f) Iron content from GeoB3313-1 core (Lamy et al., 2001); higher Fe concentrations indicate a poleward position of the southern westerly winds (SWW) and vice versa.



595 **Fig. 6-** (a) Polynya efficiency (Mezgec et al., 2017) with standard deviation values, derived from a stacked record of *F. curta* from the coastal sea ice zone of the Western Ross Sea and ssNa record from Taylor Dome (see Mezgec et al., 2017 for details). Elephant seal frequency data from Hall et al., 2006 (as reported in Mezgec et al., 2017). Sodium data from Siple Dome are also reported (Kreutz et al., 1997) (b) First principal component obtained from the 4 year-resolved ICP-MS data series

(Brightley, 2017) spanning the period 1204-1992 CE; PC1 explains 62% of the variance and is related to marine-sourced winds (see text). Green histograms refer to the number of entire *Fragilariopsis* spp. valves per Liter per year (same as in fig. SF5 c). (c) Qualitative sketch of the atmospheric circulation pattern leading to expansion of the Ross Sea Polynya and diatom transport to RICE. Arrows on the right show expansion of the RSP, increase in aeolian diatom content, decrease in dust influx and northward shift of the SWW.

605 **Data availability**

Dust and diatom data generated in this study are included in the Supplement as Table S1 and Table S2, respectively.

Supplement

The supplement related to this article is available online at XXX

Author contributions

610 SL and BD designed the study and conducted the dust and diatom analysis. GB contributed to ice core sample cutting and dust analysis. SL, DT and EM conducted the interpretation of diatom data. NB provided the ice core samples. SL and BD conducted the interpretation of all dust, diatom and paleoclimate data reported in this study and wrote the first draft of the article. All co-authors contributed to data interpretation and provided important edits and comments on subsequent drafts.

Competing interests

615 The contact author has declared that none of the authors has any competing interests.

Acknowledgements

This work is a contribution to the Roosevelt Island Climate Evolution (RICE) Program, funded by national contributions from New Zealand, Australia, Denmark, Germany, Italy, the People's Republic of China, Sweden, the UK and the USA. Logistics support was provided by Antarctica New Zealand (K049) and the US Antarctic Program. This article is an outcome of Progetto TECLA - Dipartimenti di Eccellenza 2023–2027, funded by MUR. We also acknowledge funding to support the collecting of the RICE ice core and analysis of isotope and geochemical records through the NZ Ministry of Business, Innovation and Employment (15-VUW-131, RDF-VUW1103) and GNS Science (Global Change through Time, 540GCT12).

We thank Claudio Artoni for support in the EUROCOLD laboratory, and Sofia Cerri for helping in diatom slide preparation
625 and dust analyses.

Financial support

Funding provided by MIUR – Dipartimenti di Eccellenza 2023–2027, Project TECLA, Department of Earth and
Environmental Sciences, University of Milano-Bicocca.

630 References

Allen, C. S., Thomas, E. R., Blagbrough, H., Tetzner, D. R., Warren, R. A., Ludlow, E. C., and Bracegirdle, T. J.: Preliminary
evidence for the role played by South Westerly wind strength on the marine diatom content of an Antarctic Peninsula Ice Core
(1980–2010), *Geosci.*, 10, 87, <https://doi.org/10.3390/geosciences10030087>, 2020.

635 Arrigo, K. R. and van Dijken, G. L.: Phytoplankton dynamics within 37 Antarctic coastal polynya systems, *J. Geophys. Res.-
Oceans*, 108, <https://doi.org/10.1029/2002JC001739>, 2003.

Bertler, N. A. N., Barrett, P. J., Mayewski, P. A., Fogt, R. L., Kreutz, K. J., and Shulmeister, J.: El Niño suppresses Antarctic
warming, *Geophys. Res. Lett.*, 31, L15207, <https://doi.org/10.1029/2004GL020749>, 2004.

640

Bertler, N. A. N., Naish, T. R., Mayewski, P. A., and Barrett, P. J.: Opposing oceanic and atmospheric ENSO influences on
the Ross Sea Region, Antarctica, *Adv. Geosci.*, 6, 83–86, <https://doi.org/10.5194/adgeo-6-83-2006>, 2006.

Bertler, N. A. N., Mayewski, P. A., and Carter, L.: Cold conditions in Antarctica during the Little Ice Age – Implications for
645 abrupt climate change mechanisms, *Earth Planet. Sci. Lett.*, 308, 41–51, <https://doi.org/10.1016/j.epsl.2011.05.021>, 2011.

Bertler, N. A. N., Conway, H., Dahl-Jensen, D., Emanuelsson, D. B., Winstrup, M., Vallelonga, P. T., Lee, J. E., Brook, E. J.,
Severinghaus, J. P., Fudge, T. J., Keller, E. D., Baisden, W. T., Hindmarsh, R. C. A., Neff, P. D., Blunier, T., Edwards, R.,
Mayewski, P. A., Kipfstuhl, S., Buizert, C., Canessa, S., Dacic, R., Kjær, H. A., Kurbatov, A., Zhang, D., Waddington, E. D.,
650 Baccolo, G., Beers, T., Brightley, H. J., Carter, L., Clemens-Sewall, D., Ciobanu, V. G., Delmonte, B., Eling, L., Ellis, A.,
Ganesh, S., Golledge, N. R., Haines, S., Handley, M., Hawley, R. L., Hogan, C. M., Johnson, K. M., Korotkikh, E., Lowry, D.
P., Mandeno, D., McKay, R. M., Menking, J. A., Naish, T. R., Noerling, C., Ollive, A., Orsi, A., Proemse, B. C., Pyne, A. R.,
Pyne, R. L., Renwick, J., Scherer, R. P., Semper, S., Simonsen, M., Sneed, S. B., Steig, E. J., Tuohy, A., Venugopal, A. U.,

- Valero-Delgado, F., Venkatesh, J., Wang, F., Wang, S., Winski, D. A., Winton, V. H. L., Whiteford, A., Xiao, C., Yang, J.,
655 and Zhang, X.: The Ross Sea Dipole – temperature, snow accumulation and sea ice variability in the Ross Sea region,
Antarctica, over the past 2700 years, *Clim. Past*, 14, 193–214, <https://doi.org/10.5194/cp-14-193-2018>, 2018.
- Bory, A., Biscaye, P. E., Piotrowski, A. M., and Steffensen, J. P.: Multiple sources supply aeolian mineral dust to the Atlantic
sector of coastal Antarctica: Evidence from recent snow layers at the top of Berkner Island ice sheet, *Earth Planet. Sci. Lett.*,
660 291, 138–148, <https://doi.org/10.1016/j.epsl.2010.01.006>, 2010.
- Bradley, R. S., Hughes, M. K., and Diaz, H. F.: Climate in medieval time, *Science*, 302, 404–405,
<https://doi.org/10.1126/science.1090372>, 2003.
- 665 Brightley, H. J.: A Paleoclimate Reconstruction of the Little Ice Age to Modern Era Climate Conditions in the Eastern Ross
Sea, Antarctica as Captured in the RICE Ice Core: A Thesis Submitted to the Victoria University of Wellington in Partial
Fulfilment of the Requirements for the Degree of Master of Science in Geology, MSc thesis, Victoria University of Wellington,
Wellington, New Zealand, 2017.
- 670 Bromwich, D. H. and Robasky, F. M.: Recent precipitation trends over the polar ice sheets, *Meteorol. Atmos. Phys.*, 51, 259–
274, <https://doi.org/10.1007/BF01030498>, 1993.
- Bromwich, D., Liu, Z., Rogers, A. N., and Van Woert, M. L.: Winter atmospheric forcing of the Ross Sea polynya, in: *Ocean,
Ice and Atmosphere: Interactions at the Antarctic Continental Margin*, edited by: Jacobs, S. S. and Weiss, R. F., *Antarct. Res.*
675 *Ser.*, 75, AGU, Washington, DC, 101–133, <https://doi.org/10.1029/AR075p0101>, 1998.
- Burckle, L. H., Gayley, R. I., Ram, M., and Lille, R. J.: Diatoms in Antarctic ice cores: Some implications for the glacial
history of Antarctica, *Geology*, 16, 326–329, [https://doi.org/10.1130/0091-7613\(1988\)016%3C0326:DIAICS%3E2.3.CO;2](https://doi.org/10.1130/0091-7613(1988)016%3C0326:DIAICS%3E2.3.CO;2),
1988.
- 680 Caiazzo, L., Baccolo, G., Barbante, C., Becagli, S., Bertò, M., Ciardini, V., Crotti, I., Delmonte, B., Dreossi, G., Frezzotti,
Gabrieli, J., Giardi, F., Han, Y., Hong, S. -B., Hur, S. D., Hwang, H., Kang, J. -H., Narcisi, B., Proposito, M., Scarchilli, C.,
M., Selmo, E., Severi, M., Spolaor, A., Stenni, B., Traversi, R., and Udisti, R.: Prominent features in isotopic, chemical and
dust stratigraphies from coastal East Antarctic ice sheet (Eastern Wilkes Land), *Chemosphere*, 176, 273–287,
685 <https://doi.org/10.1016/j.chemosphere.2017.02.115>, 2017.

Carrasco, J. F., Bromwich, D. H., and Monaghan, A. J.: Distribution and characteristics of mesoscale cyclones in the Antarctic: Ross Sea eastward to the Weddell Sea, *Mon. Weather Rev.*, 131, 289–301, [https://doi.org/10.1175/1520-0493\(2003\)131<0289:DACOMC>2.0.CO;2](https://doi.org/10.1175/1520-0493(2003)131<0289:DACOMC>2.0.CO;2), 2003.

690

Cefarelli, A. O., Ferrario, M. E., Almandoz, G. O., Atencio, A. G., Akselman, R., and Vernet, M.: Diversity of the diatom genus *Fragilariopsis* in the Argentine Sea and Antarctic waters: morphology, distribution and abundance, *Polar Biol.*, 33, 1463–1484, <https://doi.org/10.1007/s00300-010-0794-z>, 2010.

695 Conroy, J. L., Overpeck, J. T., Cole, J. E., Shanahan, T. M., and Steinitz-Kannan, M.: Holocene changes in eastern tropical Pacific climate inferred from a Galápagos lake sediment record, *Quat. Sci. Rev.*, 27, 1166–1180, <https://doi.org/10.1016/j.quascirev.2008.02.015>, 2008.

700 Delmonte, B., Baroni, C., Andersson, P. S., Narcisi, B., Salvatore, M. C., Petit, J. R., Scarchilli, C., Frezzotti, M., Albani, S., and Maggi, V.: Modern and Holocene aeolian dust variability from Talos Dome (Northern Victoria Land) to the interior of the Antarctic ice sheet, *Quat. Sci. Rev.*, 64, 76–89, <https://doi.org/10.1016/j.quascirev.2012.11.033>, 2013.

Delmonte, B., Páleari, C. I., Andò, S., Garzanti, E., Andersson, P. S., Petit, J. R., Crosta, X., Narcisi, B., Baroni, C., Salvatore, M. C., Baccolo, G., and Maggi, V.: Causes of dust size variability in central East Antarctica (Dome B): Atmospheric transport from expanded South American sources during Marine Isotope Stage 2, *Quat. Sci. Rev.*, 168, 55–68, <https://doi.org/10.1016/j.quascirev.2017.05.009>, 2017.

710 Delmonte, B., Winton, H., Baroni, M., Baccolo, G., Hansson, M., Andersson, P., Baroni, C., Salvatore, M. C., Lanci, L., and Maggi, V.: Holocene dust in East Antarctica: Provenance and variability in time and space, *Holocene*, 30, 546–558, <https://doi.org/10.1177/0959683619875188>, 2020.

Drucker, R., Martin, S., and Kwok, R.: Sea ice production and export from coastal polynyas in the Weddell and Ross Seas, *Geophys. Res. Lett.*, 38, L17502, <https://doi.org/10.1029/2011GL048668>, 2011.

715 Emanuelsson, B. D.: Central tropical Pacific ENSO variability preserved in water stable isotopes from the Roosevelt Island Climate Evolution (RICE) ice core, Antarctica. High-Resolution Water Stable Isotope Ice-Core Record: Roosevelt Island, Antarctica PhD Thesis, 143 pp., 2016.

- Emanuelsson, B. D., Bertler, N. A. N., Neff, P. D., Renwick, J. A., Markle, B. R., Baisden, W. T., and Keller, E. D.: The role of Amundsen–Bellingshausen Sea anticyclonic circulation in forcing marine air intrusions into West Antarctica, *Clim. Dyn.*, 51, 3579–3596, <https://doi.org/10.1007/s00382-018-4097-3>, 2018.
- Emanuelsson, B. D., Renwick, J. A., Bertler, N. A. N., Baisden, W. T., Thomas, E. R.: The role of large-scale drivers in the Amundsen Sea Low variability and associated changes in water isotopes from the Roosevelt Island ice core, *Antarctica, Clim. Dyn.*, 60, 4145–4155, <https://doi.org/10.1007/s00382-022-06589-2>, 2023.
- Fraser, A. D., Ohshima, K. I., Nishihashi, S., Massom, R. A., Tamura, T., Nakata, K., Williams, G. D., Carpentier, S., and Willmes, S.: Landfast ice controls on sea-ice production in the Cape Darnley Polynya: A case study, *Remote Sens. Environ.*, 233, 111315, <https://doi.org/10.1016/j.rse.2019.111315>, 2019.
- Fusco, G., Budillon, G., and Spezie, G.: Surface heat fluxes and thermohaline variability in the Ross Sea and in Terra Nova Bay polynya, *Cont. Shelf Res.*, 29, 1887–1895, <https://doi.org/10.1016/j.csr.2009.07.006>, 2009.
- Hall, B. L., Hoelzel, A. R., Baroni, C., Denton, G. H., Le Boeuf, B. J., Overturf, B., and Töpf, A. L.: Holocene elephant seal distribution implies warmer-than-present climate in the Ross Sea, *P. Natl. Acad. Sci. USA*, 103, 10213–10217, <https://doi.org/10.1073/pnas.0604002103>, 2006.
- Hall, B. L., Koch, P. L., Baroni, C., Salvatore, M. C., Hoelzel, A. R., de Bruyn, M., and Welch, A. J.: Widespread southern elephant seal occupation of the Victoria land coast implies a warmer-than-present Ross Sea in the mid-to-late Holocene, *Quat. Sci. Rev.*, 303, 107991, <https://doi.org/10.1016/j.quascirev.2023.107991>, 2023.
- Helama, S., Jones, P. D., and Briffa, K. R.: Dark Ages Cold Period: A literature review and directions for future research, *Holocene*, 27, 1600–1606, <https://doi.org/10.1177/0959683617693898>, 2017.
- Heinemann, G., and Klein, T.: Simulations of topographically forced mesocyclones in the Weddell Sea and the Ross Sea region of Antarctica, *Mon. Weather Rev.*, 131, 302–316, [https://doi.org/10.1175/1520-0493\(2003\)131<0302:SOTFMI>2.0.CO;2](https://doi.org/10.1175/1520-0493(2003)131<0302:SOTFMI>2.0.CO;2), 2003.
- IPCC, 2021: *Climate Change 2021: The Physical Science Basis. Contribution of Working Group I to the Sixth Assessment Report of the Intergovernmental Panel on Climate Change* Masson-Delmotte, V., Zhai, P., Pirani, A., Connors, S. L., Péan, C., Berger, S., Caud, N., Chen, Y., Goldfarb, L., Gomis, M. I., Huang, M., Leitzell, K., Lonnoy, E., Matthews, J. B. R., Maycock, T. K., Waterfield, T., Yelekçi, O., Yu, R., and Zhou, B.: *Climate Change 2021: The Physical Science Basis*.

- Contribution of Working Group I to the Sixth Assessment Report of the Intergovernmental Panel on Climate Change. Cambridge University Press, Cambridge, United Kingdom and New York, NY, USA, IPCC, 2391, 755 <https://doi.org/10.1017/9781009157896>, 2021.
- Jacobs, S. S., and Comiso, J. C.: Sea ice and oceanic processes on the Ross Sea continental shelf, *J. Geophys. Res.-Oceans*, 94, 18195–18211, <https://doi.org/10.1029/JC094iC12p18195>, 1989.
- 760 Jones, P. D., and Mann, M. E.: Climate over past millennia, *Rev. Geophys.*, 42, RG2002, <https://doi.org/10.1029/2003RG000143>, 2004.
- Kellogg, D. E., and Kellogg, T. B.: Diatoms in South Pole ice: Implications for aeolian contamination of Sirius Group deposits, *Geology*, 24, 115–118, [https://doi.org/10.1130/0091-7613\(1996\)024<0115:DISPII>2.3.CO;2](https://doi.org/10.1130/0091-7613(1996)024<0115:DISPII>2.3.CO;2), 1996.
- 765 Kellogg, D. E., and Kellogg, T. B.: Frozen in time: The diatom record in ice cores from remote drilling sites on the Antarctic ice sheets, in: *Antarctic Research Series*, Princeton University Press, Princeton, NJ, USA, 69–93, 2005.
- Kingslake, J., Hindmarsh, R. C. A., Aðalgeirsdóttir, G., Conway, H., Corr, H. F. J., Gillet-Chaulet, F., Martín, C., King, E. C., 770 Mulvaney, R., and Pritchard, H. D.: Full-depth englacial vertical ice sheet velocities measured using phase-sensitive radar, *J. Geophys. Res.-Earth Surf.*, 119, 2604–2618, <https://doi.org/10.1002/2014JF003275>, 2014.
- Klein, T., and Heinemann, G.: On the forcing mechanisms of mesocyclones in the eastern Weddell Sea region, Antarctica: Process studies using a mesoscale numerical model, *Meteorol. Z.*, 10, 113–122, [https://doi.org/10.1127/0941-2948/2001/0010-](https://doi.org/10.1127/0941-2948/2001/0010-0113) 775 0113, 2001.
- Koffman, B. G., Kreutz, K. J., Breton, D. J., Kane, E. J., Winski, D. A., Birkel, S. D., Kurbatov, A. V., and Handley, M. J.: Centennial-scale variability of the Southern Hemisphere westerly wind belt in the eastern Pacific over the past two millennia, *Clim. Past*, 10, 1125–1144, <https://doi.org/10.5194/cp-10-1125-2014>, 2014.
- 780 Kreutz, K. J., Mayewski, P. A., Meeker, L. D., Twickler, M. S., Whitlow, S. I., and Pittalwala, I. I.: Bipolar changes in atmospheric circulation during the Little Ice Age, *Science*, 277, 1294–1296, 1997.
- Lamb, H. H.: The early medieval warm epoch and its sequel, *Palaeogeogr. Palaeoclimatol. Palaeoecol.*, 1, 13–37, 785 [https://doi.org/10.1016/0031-0182\(65\)90004-0](https://doi.org/10.1016/0031-0182(65)90004-0), 1965.

Lamy, F., Hebbeln, D., Röhl, U., and Wefer, G.: Holocene rainfall variability in southern Chile: a marine record of latitudinal shifts of the Southern Westerlies, *Earth Planet. Sc. Lett.*, 185, 369–382, [https://doi.org/10.1016/S0012-821X\(00\)00381-2](https://doi.org/10.1016/S0012-821X(00)00381-2), 2001.

790

Lee, J. E., Brook, E. J., Bertler, N. A. N., Buizert, C., Baisden, T., Blunier, T., Ciobanu, V. G., Conway, H., Dahl-Jensen, D., Fudge, T. J., Hindmarsh, R., Keller, E. D., Parrenin, F., Severinghaus, J. P., Vallelonga, P., Waddington, E. D., and Winstrup, M.: An 83 000-year-old ice core from Roosevelt Island, Ross Sea, Antarctica, *Clim. Past*, 16, 1691–1713, <https://doi.org/10.5194/cp-16-1691-2020>, 2020.

795

Legrand, M., and Kirchner, S.: Polar atmospheric circulation and chemistry of recent (1957-1983) south polar precipitation, *Geophys. Res. Lett.*, 15, 879–882, <https://doi.org/10.1029/GL015i008p00879>, 1988.

Li, X., Cai, W., Meehl, G. A., Chen, D., Yuan, X., Raphael, M., Holland, D. M., Ding, Q., Fogt, R. L., Markle, B. R., Wang, G., Bromwich, D. H., Turner, J., Xie, S.-P., Steig, E. J., Gille, S. T., Xiao, C., Wu, B., Lazzara, M. A., Chen, X., Stammerjohn, S., Holland, P. R., Holland, M. M., Cheng, X., Price, S. F., Wang, Z., Bitz, C. M., Shi, J., Gerber, E. P., Liang, X., Goosse, H., Yoo, C., Ding, M., Geng, L., Xin, M., Li, C., Dou, T., Liu, C., Sun, W., Wang, X., and Song, C.: Tropical teleconnection impacts on Antarctic climate changes, *Nat. Rev. Earth Environ.*, 2, 680–698, <https://doi.org/10.1038/s43017-021-00204-5>, 2021.

805

Ljungqvist, F. C.: A new reconstruction of temperature variability in the extra-tropical Northern Hemisphere during the last two millennia, *Geogr. Ann. Ser. A-Phys. Geogr.*, 92, 339–351, <https://doi.org/10.1111/j.1468-0459.2010.00399.x>, 2010.

Lundholm, N., and Hasle, G. R.: Are *Fragilariopsis cylindrus* and *Fragilariopsis nana* bipolar diatoms?—Morphological and molecular analyses of two sympatric species. *Nova Hedwigia, Beiheft*, 133, 231-250, 2008.

810

Maffezzoli, N., Cook, E., van der Bilt, W. G. M., Støren, E. N., Festi, D., Muthreich, F., Seddon, A. W. R., Burgay, F., Baccolo, G., Mygind, A. R. F., Petersen, T., Spolaor, A., Vascon, S., Pelillo, M., Ferretti, P., dos Reis, R. S., Simões, J. C., Ronen, Y., Delmonte, B., Viccaro, M., Steffensen, J. P., Dahl-Jensen, D., Nisancioglu, K. H., and Barbante, C.: Detection of ice core particles via deep neural networks, *The Cryosphere*, 17, 539–565, <https://doi.org/10.5194/tc-17-539-2023>, 2023.

815

Mann, M. E., Zhang, Z., Rutherford, S., Bradley, R. S., Hughes, M. K., Shindell, D., Ammann, C., Faluvegi, G., and Ni, F.: Global signatures and dynamical origins of the Little Ice Age and Medieval Climate Anomaly, *Science*, 326, 1256–1260, <https://doi.org/10.1126/science.1177303>, 2009.

820

- Masson, V., Vimeux, F., Jouzel, J., Morgan, V., Delmotte, M., Ciais, P., Hammer, C., Johnsen, S., Lipenkov, V. Ya., Mosley-Thompson, E., Petit, J. R., Steig, E. J., Stievenard, M., and Vaikmae, R.: Holocene climate variability in Antarctica based on 11 ice-core isotopic records, *Quat. Res.*, 54, 348–358, <https://doi.org/10.1006/qres.2000.2172>, 2000.
- 825 Matthews, J. A., and Briffa, K. R.: The ‘Little Ice Age’: re-evaluation of an evolving concept, *Geogr. Ann. Ser. A-Phys. Geogr.*, 87, 17–36, <https://doi.org/10.1111/j.0435-3676.2005.00242.x>, 2005.
- McKay, R. M., Barrett, P. J., Harper, M. A., and Hannah, M. J.: Atmospheric transport and concentration of diatoms in surficial and glacial sediments of the Allan Hills, Transantarctic Mountains, *Palaeogeogr. Palaeoclimatol. Palaeoecol.*, 260, 168–183, 830 <https://doi.org/10.1016/j.palaeo.2007.08.014>, 2008.
- Mezgec, K., Stenni, B., Crosta, X., Masson-Delmotte, V., Baroni, C., Braida, M., Ciardini, V., Colizza, E., Melis, R., Salvatore, M. C., Severi, M., Scarchilli, C., Traversi, R., Udisti, R., and Frezzotti, M.: Holocene sea ice variability driven by wind and polynya efficiency in the Ross Sea, *Nat. Commun.*, 8, 1334, <https://doi.org/10.1038/s41467-017-01455-x>, 2017.
- 835 Morales Maqueda, M. A., Willmott, A. J., and Biggs, N. R. T.: Polynya dynamics: a review of observations and modeling, *Rev. Geophys.*, 42, RG1004, <https://doi.org/10.1029/2002RG000116>, 2004.
- Moy, C. M., Seltzer, G. O., Rodbell, D. T., and Anderson, D. M.: Variability of El Niño/Southern Oscillation activity at 840 millennial timescales during the Holocene epoch, *Nature*, 420, 162–165, <https://doi.org/10.1038/nature01194>, 2002.
- Neff, P. D., and Bertler, N. A. N.: Trajectory modeling of modern dust transport to the Southern Ocean and Antarctica, *J. Geophys. Res.-Atmos.*, 120, 9303–9322, <https://doi.org/10.1002/2015JD023304>, 2015.
- 845 O’Connor, G.K., Steig, E.J. and Hakim, G.J.: Strengthening Southern Hemisphere westerlies and Amundsen Sea low deepening over the 20th century revealed by proxy-data assimilation, *Geophys. Res. Lett.*, 48, e2021GL095999, <https://doi.org/10.1029/2021GL095999>, 2021.
- PAGES2k Consortium: A global multiproxy database for temperature reconstructions of the Common Era, *Scientific data*, 4, 850 170088, <https://doi.org/10.1038/sdata.2017.88>, 2017.
- Park, J., Kim, H.-C., Kidwell, A., and Hwang, J.: Multi-temporal variation of the Ross Sea Polynya in response to climate forcings, *Polar Res.*, 37, 1444891, <https://doi.org/10.1080/17518369.2018.1444891>, 2018.

- 855 Petit, J.-R., and Delmonte, B.: A model for large glacial–interglacial climate-induced changes in dust and sea salt concentrations in deep ice cores (central Antarctica): palaeoclimatic implications and prospects for refining ice core chronologies, *Tellus B*, 61, 768–790, <https://doi.org/10.1111/j.1600-0889.2009.00463.x>, 2009.
- Raphael, M. N., Holland, M. M., Landrum, L., and Hobbs, W. R.: Links between the Amundsen Sea Low and sea ice in the
860 Ross Sea: seasonal and interannual relationships, *Clim. Dyn.*, 52, 2333–2349, <https://doi.org/10.1007/s00382-018-4258-4>, 2019.
- Rein, B., Lückge, A., Reinhardt, L., Sirocko, F., Wolf, A., Dullo, W.-C.: El Niño variability off Peru during the last 20,000 years, *Paleoceanogr. Paleoclimat.*, 20, <https://doi.org/10.1029/2004PA001099>, 2005.
- 865 Renwick, J. A.: ENSO-related variability in the frequency of South Pacific blocking. *Monthly Weather Review* 126.12: 3117–3123. 1998.
- Rhodes, R. H., Bertler, N. A. N., Baker, J. A., Steen-Larsen, H. C., Sneed, S. B., Morgenstern, U., and Johnsen, S. J.: Little
870 Ice Age climate and oceanic conditions of the Ross Sea, Antarctica from a coastal ice core record, *Clim. Past*, 8, 1223–1238, <https://doi.org/10.5194/cp-8-1223-2012>, 2012.
- Sinclair, K. E., Bertler, N. A. N., and Trompeter, W. J.: Synoptic controls on precipitation pathways and snow delivery to high-accumulation ice core sites in the Ross Sea region, Antarctica, *J. Geophys. Res.-Atmos.*, 115, D22112,
875 <https://doi.org/10.1029/2010JD014383>, 2010.
- Smerdon, J. E., and Pollack, H. N.: Reconstructing Earth's surface temperature over the past 2000 years: the science behind the headlines, *Wiley Interdiscip. Rev.-Clim. Change*, 7, 746–771, <https://doi.org/10.1002/wcc.418>, 2016.
- 880 Steig, E. J., Morse, D. L., Waddington, E. D., Stuiver, M., Grootes, P. M., Mayewski, P. A., Twickler, M. S., and Whitlow, S. I.: Wisconsinan and holocene climate history from an ice core at Taylor dome, western Ross embayment, Antarctica, *Geogr. Ann. Ser. A-Phys. Geogr.*, 82, 213–235, <https://doi.org/10.1111/j.0435-3676.2000.00122.x>, 2000.
- Stenni, B., Curran, M. A. J., Abram, N. J., Orsi, A., Goursaud, S., Masson-Delmotte, V., Neukom, R., Goosse, H., Divine, D.,
885 van Ommen, T., Steig, E. J., Dixon, D. A., Thomas, E. R., Bertler, N. A. N., Isaksson, E., Ekaykin, A., Werner, M., and Frezzotti, M.: Antarctic climate variability on regional and continental scales over the last 2000 years, *Clim. Past*, 13, 1609–1634, <https://doi.org/10.5194/cp-13-1609-2017>, 2017.

- Stenni, B., Buiron, D., Frezzotti, M., Albani, S., Barbante, C., Bard, E., Barnola, J. M., Baroni, M., Baumgartner, M., Bonazza, M., Capron, E., Castellano, E., Chappellaz, J., Delmonte, B., Falourd, S., Genoni, L., Iacumin, P., Jouzel, J., Kipfstuhl, S., Landais, A., Lemieux-Dudon, B., Maggi, V., Masson-Delmotte, V., Mazzola, C., Minster, B., Montagnat, M., Mulvaney, R., Narcisi, B., Oerter, H., Parrenin, F., Petit, J. R., Ritz, C., Scarchilli, C., Schilt, A., Schüpbach, S., Schwander, J., Selmo, E., Severi, M., Stocker, T. F., and Udisti, R.: Expression of the bipolar see-saw in Antarctic climate records during the last deglaciation, *Nat. Geosci.*, 4, 46–49, <https://doi.org/10.1038/ngeo1026>, 2011.
- Tesi, T., Belt, S. T., Gariboldi, K., Muschitiello, F., Smik, L., Finocchiario, F., Giglio, F., Colizza, E., Gazzurra, G., Giordano, P., Morigi, C., Capotondi, L., Nogarotto, A., Köseoğlu, D., Di Roberto, A., Gallerani, A., Langone, L.: Resolving sea ice dynamics in the north-western Ross Sea during the last 2.6 ka: From seasonal to millennial timescales, *Quat. Sci. Rev.*, 237, 106299, <https://doi.org/10.1016/j.quascirev.2020.106299>, 2020.
- Tetzner, D. R., Thomas, E. R., and Allen, C.: Marine diatoms in ice cores from the Antarctic Peninsula and Ellsworth Land, Antarctica—species diversity and regional variability, *The Cryosphere Discuss.*, 2021, 1–32, <https://doi.org/10.5194/tc-2021-70>, 2021.
- Tetzner, D. R., Allen, C. S., and Thomas, E. R.: Regional variability of diatoms in ice cores from the Antarctic Peninsula and Ellsworth Land, Antarctica, *The Cryosphere*, 16, 779–798, <https://doi.org/10.5194/tc-16-779-2022>, 2022a.
- Tetzner, D. R., Thomas, E. R., Allen, C. S., and Grieman, M. M.: Regional validation of the use of diatoms in ice cores from the Antarctic Peninsula as a Southern Hemisphere westerly wind proxy, *Clim. Past*, 18, 1709–1727, <https://doi.org/10.5194/cp-18-1709-2022>, 2022b.
- Tuohy, A., Bertler, N. A. N., Neff, P. D., Edwards, R., Emanuelsson, D. B., Beers, T., and Mayewski, P. A.: Transport and deposition of heavy metals in the Ross Sea Region, Antarctica, *J. Geophys. Res.-Atmos.*, 120, 10,996–11,011, <https://doi.org/10.1002/2015JD023293>, 2015.
- Turner, J., Phillips, T., Hosking, J.S., Marshall, G.J. and Orr, A.: The Amundsen Sea Low, *Int. J. Climat.*, 33, 1818–1829, <https://doi.org/10.1002/joc.3558>, 2013.
- Turner, J., Hosking, J. S., Marshall, G. J., Phillips, T., Bracegirdle, T. L.: Antarctic sea ice increase consistent with intrinsic variability of the Amundsen Sea Low, *Clim. Dyn.*, 46, 2391–2402, <https://doi.org/10.1007/s00382-015-2708-9>, 2016.

Tianjiao, W., Wei, H., and Xiao, J.: Dynamic linkage between the interannual variability of the spring Ross Ice Shelf Polynya and the atmospheric circulation anomalies, *Clim. Dyn.*, 58, 831–840, <https://doi.org/10.1007/s00382-021-05936-0>, 2022.

- 925 Winstrup, M., Vallengaard, P., Kjær, H. A., Fudge, T. J., Lee, J. E., Riis, M. H., Edwards, R., Bertler, N. A. N., Blunier, T., Brook, E. J., Buizert, C., Ciobanu, G., Conway, H., Dahl-Jensen, D., Ellis, A., Emanuelsson, B. D., Hindmarsh, R. C. A., Keller, E. D., Kurbatov, A. V., Mayewski, P. A., Neff, P. D., Pyne, R. L., Simonsen, M. F., Svensson, A., Tuohy, A., Waddington, E. D., and Wheatley, S.: A 2700-year annual timescale and accumulation history for an ice core from Roosevelt Island, West Antarctica, *Clim. Past*, 15, 751–779, <https://doi.org/10.5194/cp-15-751-2019>, 2019.

930

Winton, V. H. L., Edwards, R., Delmonte, B., Ellis, A., Andersson, P. S., Bowie, A., Bertler, N. A. N., Neff, P., and Touhy, A.: Multiple sources of soluble atmospheric iron to Antarctic waters, *Glob. Biogeochem. Cycles*, 30, 421–437, <https://doi.org/10.1002/2015GB005265>, 2016a.

- 935 Winton, V. H. L., Dunbar, G. B., Atkins, C. B., Bertler, N. A. N., Delmonte, B., Andersson, P. S., Bowie, A., and Edwards, R.: The origin of lithogenic sediment in the south-western Ross Sea and implications for iron fertilization, *Antarct. Sci.*, 28, 250–260, <https://doi.org/10.1017/S0954102016000153>, 2016b.

- Wolff, E. W., Barbante, C., Becagli, S., Bigler, M., Boutron, C. F., Castellano, E., de Angelis, M., Federer, U., Fischer, H., 940 Fundel, F., Hansson, M., Hutterli, M., Jonsell, U., Karlin, T., Kaufmann, P., Lambert, F., Littot, G. C., Mulvaney, R., Röthlisberger, R., Ruth, U., Severi, M., Siggaard-Andersen, M. L., Sime, L. C., Steffensen, J. P., Stocker, T. F., Traversi, R., Twarloh, B., Udisti, R., Wagenbach, D., and Wegner, A.: Changes in environment over the last 800,000 years from chemical analysis of the EPICA Dome C ice core, *Quat. Sci. Rev.*, 29, 285–295, <https://doi.org/10.1016/j.quascirev.2009.06.013>, 2010.

- 945 Yan, H., Sun, L., Wang, Y., Huang, W., Qiu, S., and Yang, C.: A record of the Southern Oscillation Index for the past 2,000 years from precipitation proxies, *Nat. Geosci.*, 4, 611–614, <https://doi.org/10.1038/ngeo1231>, 2011.

Yiu, Y. Y. S., and Maycock, A. C.: The linearity of the El Niño teleconnection to the Amundsen Sea region, *Q. J. R. Meteorol. Soc.*, 146, 1196–1211, <https://doi.org/10.1002/qj.3731>, 2019.

950

Yokoyama, Y., Anderson, J. B., Yamane, M., Simkins, L. M., Miyairi, Y., Yamazaki, T., Koizumi, M., Suga, H., Kusahara, K., Prothro, L., Hasumi, H., Southon, J. R., and Ohkouchi, N.: Widespread collapse of the Ross Ice Shelf during the late Holocene, *P. Natl. Acad. Sci. USA*, 113, 2354–2359, <https://doi.org/10.1073/pnas.1516908113>, 2016.

955 Zhang, C., Li, T., and Li, S.: Impacts of CP and EP El Niño events on the Antarctic sea ice in austral spring, *J. Clim.*, 34,
9327–9348, <https://doi.org/10.1175/JCLI-D-21-0002.1>, 2021.

Zwally, H. J., Comiso, J. C., and Gordon, A. L.: Antarctic offshore leads and polynyas and oceanographic effects, in:
Oceanology of the Antarctic continental shelf, *Antarct. Res. Ser.*, 43, 203–226, <https://doi.org/10.1029/AR043p0203>, 1985.

960